NASA TECHNICAL NOTE

NASA TN D-5307

C. 1

TECH LIBRARY KAFB, NM
0132173

NASA TN D-5307

LOAN COPY: RETURN TO
AFWL (WLIL-2)
KIRTLAND AFB, N MEX

DRAG REDUCTION DUE TO GAS INJECTION THROUGH VARIOUS DISCRETE SLOTS ON A THREE-DIMENSIONAL WING AT MACH 2.01

by Russell B. Sorrells III, K. R. Czarnecki, and Lorraine F. Satchell

Langley Research Center
Langley Station, Hampton, Va.

NATIONAL AERONAUTICS AND SPACE ADMINISTRATION • WASHINGTON, D. C. • JULY 1969

TECH LIBRARY KAFB, NM
0132173

DRAG REDUCTION DUE TO GAS INJECTION THROUGH VARIOUS DISCRETE SLOTS ON A THREE-DIMENSIONAL WING AT MACH 2.01

By Russell B. Sorrells III, K. R. Czarnecki, and Lorraine F. Satchell

Langley Research Center
Langley Station, Hampton, Va.

NATIONAL AERONAUTICS AND SPACE ADMINISTRATION

For sale by the Clearinghouse for Federal Scientific and Technical Information
Springfield, Virginia 22151 – CFSTI price $3.00

DRAG REDUCTION DUE TO GAS INJECTION THROUGH VARIOUS DISCRETE SLOTS ON A THREE-DIMENSIONAL WING AT MACH 2.01

By Russell B. Sorrells III, K. R. Czarnecki,
and Lorraine F. Satchell
Langley Research Center

SUMMARY

Force measurements were made of the drag reduction due to the injection of gas into a turbulent boundary layer through discrete slots of various sizes and configurations on a three-dimensional semispan wing at a Mach number of 2.01. Air, helium, and Freon were injected, transition was fixed, and the tests were conducted at Reynolds numbers, based on the mean geometric chord, ranging up to 4.48×10^6. The theoretically estimated and measured skin-friction reductions are compared.

The results indicate the possibility of effects due to local distortions of the boundary layer for injection through discrete slots as well as porous surfaces; therefore, extrapolation of low Reynolds number data for discrete slots to full-scale Reynolds number values is not possible. Consequently, it appears that theoretical assumptions are more consistent with actual flight conditions than with wind-tunnel conditions on small-chord wings. It was found that for the supersonic transport and for the slot drags incurred in this investigation, engine bleed air does not provide sufficient mass flow to warrant the use of air injection for drag reduction over an entire wing span. However, if the engine bleed air is injected only over the nacelles, it appears possible at Mach 2.0 to achieve a drag reduction equivalent to from 9 to 35 percent of the nacelle skin friction, the percentage depending on the amount of bleed plenum pressure energy that is used for thrust. Full recovery of the energy in the bleed plenum air amounts to an equivalent reduction in nacelle skin friction of 65 percent. Greater drag reductions were obtained by injecting helium into the boundary layer than by injecting air or Freon, but calculations show that for a typical high-performance supersonic transport, the increase in drag due to lift caused by the extra weight of the helium is greater than the skin-friction reduction. The smallest rounded-shoulder slot achieved the greatest net drag reduction, but for a given slot size the sharp-shoulder slots, the screens, and the perforated plates seem to have the lowest slot drag. In the design of an ejection system, the slot drag and the available thrust rather than the skin-friction reduction should be optimized, and the possible lift interference effects of an injected gas should be considered in selecting the location of an ejection slot or nozzle.

INTRODUCTION

Since the skin-friction drag is a significant part of the total drag of a supersonic aircraft, the development of feasible methods of reducing it is of current interest. One method of reducing the turbulent boundary-layer skin friction is to inject low-velocity gas into the boundary layer. Engine bleed air or spent cabin air can serve as a source of this low-velocity gas. Gas can be injected into the boundary layer through a porous surface over the entire surface area of interest or through discrete slots.

The first method has been studied in detail (refs. 1 to 8), but little has been done to investigate the potential gains of the second method (refs. 7 and 8), although it may be more practical.

The reduction in skin friction for both methods is achieved by the forced thickening of the boundary layer (a thicker boundary layer of the same basic profile has a lower velocity gradient at the surface) and by the distortion of the boundary-layer profile, which results in a lower velocity gradient at the surface. The extent to which boundary-layer distortion is a factor in discrete slot injection, however, depends upon how quickly the injected gas reaches equilibrium with the boundary layer.

The purpose of this investigation was to determine the amount of drag reduction possible by means of gas injection through a discrete slot and to determine the accuracy of the theory presented in reference 9. Slots of various sizes and configurations were tested on a trapezoidal wing with a symmetrical hexagonal section. Force data were taken at a Mach number of 2.01 at angles of attack from -5° to 5° through a range of gas-injection mass-flow rates. Air was the principal gas used for injection, but helium and Freon were also used. Transition was fixed and the tests were conducted primarily at a Reynolds number of 3.36×10^6, based on the mean geometric chord; however, some tests were made at Reynolds numbers of 2.02×10^6 and 4.48×10^6. The skin-friction reductions are compared with the theoretical estimates of skin-friction reduction from reference 9.

SYMBOLS

The units for the physical quantities defined in this paper are given both in the U.S. Customary Units and in the International System of Units (SI). Factors relating the two systems are given in reference 10.

c local chord

$\bar{c}$ mean geometric chord, 10.889 inches (27.658 centimeters)

C_D measured drag coefficient, $\frac{\text{Drag}}{q_\infty S}$

$\Delta C_{D,F}$ skin-friction reduction, $C_D - (C_D)_{\dot{m}=0} - C_{T,D}$

$\Delta C_{D,N}$ net drag reduction, $C_D - C_{D,s}$

C_F theoretical smooth-wing skin-friction coefficient based on wing planform area

C_L lift coefficient, $\frac{\text{Lift}}{q_\infty S}$

$C_{L,N}$ net aerodynamic lift coefficient, $(C_L)_{\dot{m}=0} + C_{T,L}$

$C_{T,D}$ thrust coefficient in drag direction, $\frac{T_D}{q_\infty S}$

$C_{T,L}$ thrust coefficient in lift direction, $\frac{T_L}{q_\infty S}$

D_i total aircraft drag with helium injection

D_o total aircraft drag without helium injection

L/D lift-drag ratio, $\frac{C_L}{C_D}$

m_{He} total mass of helium

$\dot{m}$ injection mass-flow rate

$\frac{\dot{m}}{\dot{m}_\infty}$ mass-flow ratio, $\frac{\dot{m}}{\rho_\infty u_\infty S}$

q_∞ free-stream dynamic pressure

$R_{\bar{c}}$ Reynolds number based on free-stream conditions and mean geometric chord

r_i range with helium injection

r_o range without helium injection

S wing semispan planform area, 0.766 foot^2 (0.0712 meter^2)

T_D thrust in drag direction

T_L thrust in lift direction

u_∞ free-stream velocity

w slot width

α angle of attack

ρ_∞ free-stream density

Subscripts:

$\dot{m}=0$ zero mass-flow conditions

s smooth wing

∞ free-stream conditions

APPARATUS AND METHODS

Models and Model Mounting

The model is basically a trapezoidal semispan wing with a 4.3-percent thick symmetrical hexagonal section and with a mean geometric chord $\bar{c}$ of 10.889 in. (27.658 cm). (See fig. 1.) A hexagonal wing section was selected so that the experimental results at $\alpha = 0^\circ$ would be as comparable as possible with the theoretical skin-friction reduction on a flat plate as predicted by reference 9. Furthermore, the theory assumes that the exit pressure of the injected gas is equal to free-stream pressure and the hexagonal section should provide a slot-exit pressure very near free-stream pressure at $\alpha = 0^\circ$. The hexagonal section also simplified the measurement of the zero-lift pressure drag. Injection slots were provided on both the upper and lower surfaces of the wing. In order to obtain a uniform spanwise mass-flow rate, the interior of the wing was designed so that the injected air would pass through a series of plenums before reaching the injection slot.

The wing was attached to a four-component strain-gage balance housed within the boundary-layer bypass plate as shown in figure 2. The wing was mounted through, but not attached to, a half-body which was mounted on the boundary-layer bypass plate so that the

strain-gage balance measured the aerodynamic forces and moments on the wing only. A turntable contained in the bypass plate allowed the model to be rotated through a range of angles of attack. The flexible air supply tube was supported by the bypass plate so that there would be a minimum of fouling between the air supply tube and the wing. In order that various sizes and configurations of slots could be tested, the model was provided with removable cover plates and cover-plate inserts which formed the rear edge of the slot. Figure 2 also shows the pressure orifice locations and the stations where the wake momentum surveys were made.

The three basic slot configurations are illustrated in figure 3, where w indicates how the slot width is measured. The sharp-shoulder slots are illustrated in figure 3(a) and have a sharp corner, or shoulder, at the rear edge of the slot where the injected gas turns onto the wing surface. The rounded-shoulder slots (fig. 3(b)) have a rounded corner at this point, and the gas is injected somewhat more downstream than for the sharp-shoulder slots. Figure 3(c) illustrates the slots which were covered with wire-mesh screens and perforated plates. The gas was injected normal to the wing surface for this type of slot. Various types of wire mesh were used for the screens. The 100×100 per in^2 (39.4×39.4 per cm^2) wire mesh was 42 percent open, whereas the 80×700 per in^2 (31.5×275.6 per cm^2) wire mesh and the Monel cloth were not translucent and, consequently, were only slightly porous. The perforated plates were 29 percent open with 0.032-in.-diameter (0.081-cm) holes. As shown in figure 3, the porosity of the screens and plates was not considered in determining the slot width. All three basic types of slots were flush with the wing surface. The reference smooth wing was obtained by placing solid plates in the wing slots shown in figure 3(c).

Tests and Procedures

All tests were conducted in the Langley 4- by 4-foot supersonic pressure tunnel at a Mach number of 2.01. The tests were conducted primarily at a Reynolds number of 3.36×10^6, based on the mean geometric chord, but some tests were made at Reynolds numbers of 2.02×10^6 and 4.48×10^6. The tunnel stagnation temperature was 560° R (311° K) and the stagnation temperature of the injected gas was approximately 530° R (294° K).

Transition was fixed 0.5 inch (1.27 cm) from the wing leading edge by using No. 60 carborundum grains sparsely distributed over a 0.25-inch-wide (0.64-cm) band. Angle of attack was set by manual rotation of the turntable for visual alinement of scribe marks. All the configurations were tested at angles of attack up to 5°. All configurations were tested through a range of gas-injection mass-flow rates. Air was the principal gas used for injection, but helium and Freon were also used.

Force and moment data were taken by means of a four-component strain-gage balance and a venturi was used to measure the mass flow through the slots. Measurements

were made of venturi total pressure, differential pressure, and total temperature in order to calculate the mass-flow rate of the injected gas. Surface-pressure measurements were read from manometer boards. Wake-momentum surveys were taken, but when the calculated injected momentum thickness was subtracted from the total measured momentum thickness, negative skin-friction coefficients were obtained. This result indicated that the measured momentum thickness was incorrect.

In order to estimate the effect of tunnel static pressure on the thrust coefficients which resulted from the injected gas, force-data calibrations were made at zero Mach number for each slot configuration at several tunnel pressures. It was found that the thrust coefficients resulting from the injected gas varied with the tunnel pressure, the mass-flow ratio, and the slot configuration. Since the simulation of Reynolds numbers lower than 3.36×10^6 at Mach 0 was difficult, the calibrated thrust coefficients were extrapolated to obtain the thrust coefficient for each data point at the exact test-section static pressure at which that data point was taken. Since the wing section was hexagonal, the ambient pressure at the slot should be close to the test-section static pressure at zero lift; therefore, the extrapolation to obtain thrust coefficients for the $R_{\overline{c}} = 3.36 \times 10^6$ data is believed to be reasonably accurate; however, since the thrust coefficients begin to increase rapidly with decreasing tunnel pressure at pressures around those which simulate $R_{\overline{c}} = 3.36 \times 10^6$, the accuracy of the extrapolation for the data taken at $R_{\overline{c}} = 2.02 \times 10^6$ is not known. Most of the data for the present tests were taken at $R_{\overline{c}} = 3.36 \times 10^6$.

Accuracy

The force-data results presented in this report represent a compilation of data taken during four separate tests, tests 200, 220, 280, and 300. Figure 4 shows the lift-drag data of the smooth wing measured with the 403-S balance during tests 220 and 280 and with the 404-S balance during test 300. The reason for the difference in drag level between the values measured by the 403-S and 404-S balances is not known, but the 404-S is less sensitive than the 403-S. The smooth-wing data for each test were used as the reference data for the force data presented in figure 5. Since there were no smooth-wing data taken during test 200, an estimate of the smooth-wing drag level for this test was made by taking the increment between the zero-mass-flow drag of a slot configuration measured during test 200 and the zero-mass-flow drag of the same slot configuration measured again during test 280 and deducting this increment from the smooth-wing drag measured during test 280. This approximation is believed to be reasonably accurate for the $\alpha = 0^o$ drag, but for the angle-of-attack drag the approximated values are greater than the zero-mass-flow measured drag of most of the slotted configurations (for example, see figs. 5(d) and 5(f)). Although an error in the drag of the smooth wing will introduce an error into the absolute level of the net drag reduction, the measured drag reduction with increasing mass

flow will remain valid. Comparison of the lift-drag data for test 280 with the air supply tube both in and out indicates that there was little fouling between the air supply tube and the model. (See fig. 4.) A check on the accuracy of the data was obtained by comparing the measured minimum drag coefficient (0.0238) with the drag coefficient obtained by adding the measured pressure drag coefficient to the theoretical skin-friction coefficient obtained by the method of reference 11 (0.0240). The data in figure 4 also indicate that the repeatability was good.

PRESENTATION OF RESULTS

Results of the present investigation are presented as follows:

RESULTS AND DISCUSSION

Data Reduction Ratios

The results of the force tests are shown in figure 5. The drag reduction ratios are presented in the form of two different parameters. The first parameter, the net drag reduction ratio, is defined by the equation

$$\frac{\Delta C_{D,N}}{C_F} = \frac{C_D - C_{D,s}}{C_F} \tag{1}$$

where C_D is the measured drag coefficient of the slotted configuration, $C_{D,s}$ is the measured drag coefficient of the smooth wing, and C_F is the theoretical smooth-wing skin-friction coefficient predicted by the method of reference 11. (The values used for C_F were 0.0059, 0.0055, 0.0052 for $R_{\bar{c}} = 2.02 \times 10^6$, 3.36×10^6, and 4.48×10^6, respectively.) This parameter is a measure of the zero-mass-flow slot drag and the extent to which the beneficial effects of skin-friction reduction and the thrust of the injected gas can overcome the slot drag.

The second parameter presented in figure 5 is the skin-friction reduction ratio, which is defined by the equation

$$\frac{\Delta C_{D,F}}{C_F} = \frac{C_D - (C_D)_{\dot{m}=0} - C_{T,D}}{C_F} \tag{2}$$

where $(C_D)_{\dot{m}=0}$ is the measured drag of the slot configuration at zero mass flow and $C_{T,D}$ is the thrust coefficient in the drag direction. This parameter, which will always be zero when the mass-flow ratio is zero, is a measure of the skin-friction reduction. However, it only approximates the skin-friction reduction since it assumes that the slot drag does not change with increasing mass flow, whereas in reality the injected gas acts as a source and reduces the slot drag. In figure 5 this parameter is compared with the theoretical skin-friction reduction predicted in reference 9. The theoretical mass-flow ratio required for sonic exit velocity is also shown for the narrower slots where sonic velocities are obtained.

Thrust Coefficients

The thrust coefficient $C_{T,D}$ at any given mass-flow ratio can be read indirectly from figure 5 as the change in the difference between $\frac{\Delta C_{D,N}}{C_F}$ and $\frac{\Delta C_{D,F}}{C_F}$ from zero mass flow to the given mass-flow ratio. The thrust coefficients for the configurations with the slots and for those with the $w = 0.026c$ perforated plates are relatively large compared with the amount of skin-friction reduction obtained for these same configurations, whereas the thrust coefficients for the configurations with the screens and the $w = 0.116c$ perforated plate are zero. (See fig. 5.)

For angle-of-attack data, Mach 0 and Mach 2.01 thrust coefficients are believed to differ. Thrust coefficients increase exponentially with decreasing tunnel pressure. Consequently, when the wing is at an angle of attack, the thrust on the low-pressure side of the wing will increase more than the thrust on the high-pressure side decreases. This net increase in thrust coefficient could explain the consistently higher drag reduction indicated by the data at an angle of attack. It is believed, however, that the $\alpha = 0^o$ thrust coefficients at Mach 0 are reasonably accurate up to a mass-flow ratio about 0.003. However, since these coefficients were not obtained at Mach 2.01, it is not known for certain that they will be completely accurate.

It is evident that some of the data will be more meaningful than others. In general, the skin-friction reduction ratios are not affected by the approximated values for the smooth-wing drag of test 200, nor are they directly affected by the difference in drag level measured by the different balances. However, because of the inaccuracy of the thrust coefficients at angle of attack and of an apparent inability to correctly extrapolate for the thrust coefficients at mass-flow ratios above 0.003, the most meaningful data for skin-friction reduction are the $\alpha = 0^o$ screen data, for which the thrust coefficients are zero, and the $\alpha = 0^o$ slot and perforated-plate data at mass-flow ratios below 0.003. The net drag reduction ratio is not affected by inaccurate estimates of the thrust coefficients nor is it directly affected by the difference in the drag level measured by the two balances.

Therefore, it is meaningful for all but the test 200 angle-of-attack data, where the approximated values for smooth-wing drag are used, and even for those data the trends are valid.

Skin-Friction Reduction Ratios and Theoretical Comparisons

In figure 5 the skin-friction reduction ratios for the air injection tests are compared with the theoretical skin-friction reduction ratios predicted by reference 9. The theoretical curves in figure 5 apply to all test Reynolds numbers presented. Although the theory predicts a slight decrease in the skin-friction reduction with increasing Reynolds number, the difference for the three test Reynolds numbers presented in figure 5 is not discernible at that scale.

Since the theoretical skin-friction reduction is dependent upon the component of the injection velocity in the stream direction, the angle of injection was calculated for each slot so that this velocity component could be determined. This angle was determined by comparing the measured thrust coefficients and the thrust coefficients calculated from the mass-flow rates. For the screens and perforated plates, the velocity component in the stream direction was assumed to be zero. The variation of the stream component of the injection velocity for the configurations tested had only a small effect on skin-friction reduction at the lower mass flows; however, an increase in this stream component causes a gain in thrust that more than offsets the consequent loss in skin-friction reduction. (See fig. 5(a).)

The data shown in figure 5 usually indicate greater skin-friction reductions than are predicted by theory. The discrepancy between theoretical and measured values is thought to be caused by several factors. First, the Mach 0 thrust coefficients are believed to be in error for the angle-of-attack data and for mass-flow ratios above 0.003. Second, the slot drag is reduced with increasing mass flow because of the source strength of the injected gas. Last, the injected gas does not assume an equilibrium profile shape with the boundary layer immediately upon entering the boundary layer as the theory assumes it does; consequently, the injected gas remains at the surface of the model for a period and results in reduced local shear forces. The primary cause of the discrepancy between theoretical and measured values for the $\alpha = 0^{\circ}$ data is not believed to be the erroneous thrust coefficients, since the thrust coefficients for the screens are zero at $\alpha = 0^{\circ}$ and this discrepancy is present for the screen data. However, the irregular shape of the curves of the skin-friction reduction ratio for the rounded-shoulder slots, shown in figures 5(a), 5(b), and 5(c), indicates that the thrust coefficients are probably in error above an $\dot{m}/\dot{m}_{\infty}$ of about 0.003. This error is probably due to the fact that the extrapolation of the thrust coefficients to tunnel static pressure values becomes hazardous at the higher mass flows for these slots.

To study the slot drag reduction due to the source strength of the injected gas, attention should be directed to the $\alpha = 0^{\circ}$ data for the screens. (See figs. 5(k) to 5(r).) For

these data the thrust coefficients are zero at $\alpha = 0^{o}$ and, consequently, are not a complicating factor. The majority of these data have $\frac{\Delta C_{D,N}}{C_F}$ values which either become coincident with or pass below the theoretical curve. This trend indicates that the slot drag is appreciably reduced by the source effects; however, it does not seem reasonable that the source effects could completely negate the slot drag as some of the data indicate. Consequently, it must be concluded that the boundaty-layer distortion effects must also be a factor in producing the greater than anticipated skin-friction reductions.

Further evidence of the boundary-layer distortion effects can be seen in the Reynolds number comparisons of figures 5(b), 5(e), and 5(h). The theory (ref. 9) predicts a slight decrease in the skin-friction reduction with increasing Reynolds number, but the present data indicate an opposite trend. This opposite trend is not possibly due to erroneous Mach 0 thrust coefficients, since the net drag reduction ratios, which include Mach 2.01 thrust coefficients at the higher Reynolds numbers are greater or at least equal to the net drag reduction ratios at the lower Reynolds numbers in spite of the fact that the thrust coefficients are higher at the lower Reynolds numbers. This phenomenon could be due, however, to local boundary-layer distortion effects, or to mixing effects. Reference 7 also indicates the importance of mixing effects. If these distortion effects are present, extrapolation of the low Reynolds number data for discrete slots to full-scale Reynolds number values is not possible. The distortion effects would probably not be as significant on a full-scale aircraft because the chord lengths would probably be large enough for the assumption of immediate equilibrium between the injected gas and the boundary layer to be valid. Thus, it appears that the assumptions in the theory are more consistent with the flight conditions than with wind-tunnel conditions on small wings.

Zero-mass-flow slot drags.- It is apparent from the foregoing discussion of the net drag reduction ratio that the slot drag is an important design concern. The slot drag at mass flow cannot be determined accurately, since it decreases with increasing mass flow because of the source effects of the injected gas. However, a relative comparison of the slot drags can be made from the net drag reduction ratios at zero mass flow. These values are presented in figure 6 for $\alpha = 0^{o}$. The scatter shown for the $w = 0.026c$ screens is believed to be caused in part by the difference in surface roughness of the various screen installations.

When w/c for the screens and perforated plates shown in figure 6 is adjusted to account for the various porosities, the screens and the perforated plates appear to have about the same drag for a given slot size as the sharp-shoulder slots within the accuracy of the data. However, since this investigation does not consider the pressure losses which would undoubtably be greater for the screens and perforated plates, it appears that the sharp-shouldered slots are preferable. The drag on the sharp-shoulder slot is probably lower because the flow-reattachment point on the sharp-shoulder slot is located on the

upper corner of the slot shoulder at the surface of the wing, whereas the flow reattachment point on the rounded-shoulder slot is located on the rounded shoulder.

Net drag reduction ratios and their applications.- The net drag reduction ratios presented in figure 5 indicate that the rounded-shoulder slots (see figs. 5(a) to 5(c)) provide the greatest overall drag reductions. This appears to be primarily due to the fact that the air was injected more directly downstream and consequently provided more thrust.

This thrust appears to be realizable on a full-scale aircraft up to a mass-flow ratio of roughly 0.0024 for the data shown in figure 5(a). This conclusion is based on the assumption that only inlet bleed air will be used as the injected air and on the fact that the pressure recovery factor (0.4) measured in the model plenum at a mass-flow ratio of 0.0024 is approximately equal to that obtained in the bleed-air plenum in the inlet center body of a supersonic transport at Mach number 2.7 when the center-body boundary layer is bled off by using ram scoops.

The magnitude of the thrust provided by the ejection of air through these slots suggests that for a given quantity of gas which must be ejected and which has a given amount of energy, the greatest net drag reductions can be achieved by utilizing the available thrust rather than dissipate the energy of the gas to achieve a skin-friction reduction. Even for the best case tested, that is, the $\alpha = 5^{\circ}$ data in figure 5(a), a mass-flow ratio of 0.00025 is required just to negate the slot drag. In order to better understand what this mass-flow ratio means in terms of a full-scale aircraft the following analysis is presented:

At an altitude of 47 000 ft (14 326 m) a supersonic transport reaches Mach number 2.0 in its flight profile and attains an engine mass-flow rate of 412 lb/sec (1833 N/sec). Based on a semispan planform area of 3789 ft^2 (352.0 m^2), this mass-flow rate is equivalent to a mass-flow ratio of 0.0038. Assuming a bleed-to-inlet mass-flow ratio of 0.05, the mass-flow ratio available from the bleed air of the two engines on the semispan wing is 0.00038. At $R_{\bar{c}} = 3.36 \times 10^6$ the tunnel static pressure simulates the atmospheric pressure at 47 000 ft (14 326 m) so that, neglecting any differences in temperature ratio between engine bleed air and the air injected in these tests, the drag reductions shown in figure 5 at an $\dot{m}/\dot{m}_{\infty}$ of 0.00038 should be comparable with those obtainable on the supersonic transport at the same mass-flow ratio. A net drag reduction for air injection at an $\dot{m}/\dot{m}_{\infty}$ of 0.00038 was obtained only for the slot with $w = 0.004c$ at $\alpha = 5^{\circ}$ (fig. 5(a)). This drag reduction resulted in a 4-percent reduction in skin friction. If the theory of reference 9 is used to estimate the skin-friction reduction obtainable, then a net drag reduction does not appear possible at an $\dot{m}/\dot{m}_{\infty}$ of 0.00038 unless some means is found of reducing the slot drag. A net drag reduction could be obtained, however, by operating at a higher mass-flow ratio. A higher ratio could be obtained by either providing more injection air or by concentrating the available air over a smaller area. Further bleeding from the engine to supply additional air would not be practical, but some additional air

might be provided from ram-air turbines used to supply auxiliary power. Also, fighter aircraft with their traditionally high thrust-to-weight ratios would have relatively more bleed air. One possibility for concentrating the available mass flow over a small area would be to inject the bleed air only over the nacelle surface.

For a nacelle wetted area of 600 ft^2 (55.7 m^2), the mass-flow ratio from the bleed air of one engine would be equivalent to a mass-flow ratio of 0.00242 as defined in figure 5 where the reference area is one-half the wetted area. If it is assumed that the theoretical skin-friction reduction is more meaningful on a full-scale aircraft, it appears from the theoretical curves in figure 5 that injecting air only over the nacelle would result in a 13-percent reduction in the nacelle skin friction for a zero-thrust model (see fig. 5(p)). The lowest slot drag measured (fig. 5(p)) in terms of $\frac{\Delta C_{D,N}}{C_F}$ was 0.04; therefore, it appears that roughly the equivalent of a 9-percent reduction in the nacelle skin friction is attainable. The $\alpha = 0^o$ data of figure 5(a) indicate that for a slot designed to provide thrust by using the pressure energy of the bleed air, the equivalent of a 35-percent reduction in the nacelle skin friction is attainable at a mass-flow ratio of 0.00242. (This estimate neglects any reduction of boundary-layer distortion for a full-scale aircraft.) This compares with a maximum potential thrust equivalent to a 65-percent nacelle skin-friction reduction for a mass-flow ratio of 0.00242 and a recovery factor of 0.4 when the bleed plenum air is accelerated to free-stream pressure, assuming no skin-friction reduction. At a cruise Mach number of 2.7 at an altitude of 65 000 ft (19 812 m), the available mass-flow ratio from engine bleed air will be 0.00324 for each nacelle. From the theoretical values in figure 5, this higher mass-flow ratio will result in a further reduction in the nacelle skin friction of 2 percent; however, reference 9 indicates for a given mass-flow ratio the skin-friction reduction at Mach 2.7 is roughly 2-percent less than that at Mach 2.0. The increased bleed air at Mach 2.7 could provide more thrust. The $\alpha = 0^o$ data of figure 5(a) indicate that at a mass-flow ratio of 0.00324 a drag reduction equivalent to roughly 50 percent of the nacelle skin friction is attainable.

Foreign-gas injection and applications.- The results of the foreign-gas injection are shown in figures 5(d), 5(h), 5(j), and 5(k). The drag reductions obtained from helium injection are considerably greater than those obtained from air or Freon at a given mass-flow ratio, but calculations show that even for the best case (fig. 5(h)), where a 10-percent skin-friction reduction was obtained at a mass-flow ratio of only 0.00005, helium injection is not practical. The calculations were made for a typical high-performance supersonic transport with the following assumptions:

1. Planform area (2S) = 7578 ft^2 (704.1 m^2).

2. Mach number = 2.0.

3. Range = 4000 n. mi. (1 n. mi. = 1.852 km).

4. Altitude = 47 000 ft (14 326 m).

5. Gross weight (excluding helium) = 660 000 lb (2.936 MN).

6. Fuel and helium consumption rate is constant over the 4000 n. mi. flight.

7. Initial fuel load = 330 000 lb (1.468 MN).

8. Additional structural weight required for carrying helium is neglected.

It was found that a 10-percent reduction in skin friction will result in a 1650-lb (7339-N) skin-friction drag reduction. However, it was found that for a mass-flow ratio of 0.00005, a total of 123 800 lb (0.551 MN) of helium will be required. After 2000 n. mi. of flight, the 61 800 lb (0.275 MN) of helium carried at that point results in an additional drag due to lift of 2128 lb (9465 N). Consequently, it does not appear that a net drag reduction can be obtained by using helium. Even after neglecting the increase in drag due to lift so that a net drag reduction can be assumed, further calculations based on total energy relations given by

$$D_o r_o = D_i r_i + \frac{1}{2} m_{He} u_\infty^2 \tag{3}$$

indicate that for a fuel consumption of $1.6 \frac{\text{lb/lb}}{\text{hr}} \left(1.6 \frac{\text{N/N}}{\text{hr}}\right)$, a given weight of fuel will increase the range seven times as much as an equal weight of helium.

Lift coefficients.- The variation of the lift coefficient C_L and the net aerodynamic lift coefficient $C_{L,N}$ with mass-flow ratio is also presented in figure 5. The following equation defines $C_{L,N}$:

$$C_{L,N} = \left(C_L\right)_{\dot{m}=0} + C_{T,L} \tag{4}$$

where $C_{T,L}$ is the measured Mach 0 thrust coefficient in the lift direction. The net aerodynamic lift coefficient $C_{L,N}$ is presented only for the $\alpha = 0^o$ and $R_{\overline{c}} = 3.36 \times 10^6$ data because of the greater accuracy of the thrust coefficients at these conditions. The lift coefficient C_L does not change appreciably with mass flow for the tests where identical slots are on the top and bottom of the model, but substantial changes occurred in some configurations where the slots were different. Comparing the $C_{T,L}$ values $\left(C_{L,N} - \left(C_L\right)_{\dot{m}=0}\right)$ with the variation in C_L with mass flow indicates that depending on the slot configuration, the C_L changes vary from 2 to 13 times the values of $C_{T,L}$. Apparently, the injected gas acts as a source which causes a compression of the flow and, thereby, provides a net lifting force to the side of the model with the greatest mass flow. The magnitude of these apparent lift-interference effects suggests that they should be considered in selecting the location of an ejection slot or nozzle on an aircraft, especially when high mass-flow rates are available. Engine bypass air, for example, could provide favorable interference effects if it is ejected at the right location.

Figure 7 indicates that increases in L/D occur when more air is ejected from the underside of a wing than from the upperside. By using the supersonic transport engines again as an applications example, the 0.00038 mass-flow ratio available from engine bleed air is found to increase the maximum L/D to about 4.93 from the zero-mass-flow maximum L/D of 4.89. Lift-drag data at various mass flows were not taken for the other models with different sized slots on top and bottom, but since the lift-interference effects appear to be the weakest for the slot configuration shown in figure 7 (see fig. 5(h)), larger L/D increases might be possible with some of the other slot arrangements. However, none of the configurations achieved an L/D greater than that of a smooth wing at a mass-flow rate of 0.00038.

CONCLUSIONS

Force measurements were made of the drag reduction due to gas injection through discrete slots of various sizes and configurations on a three-dimensional semispan wing at a Mach number of 2.01 and at Reynolds numbers, based on the mean geometric chord, ranging to 4.48×10^6. The following results were obtained:

1. Results indicate the possibility of effects due to local distortions of the boundary layer for injection through discrete slots as well as porous surfaces, and therefore extrapolation of the low Reynolds number data for discrete slots to full-scale Reynolds number values is not possible. Consequently, it appears that the theoretical assumptions are more consistent with the flight conditions than with the wind-tunnel conditions on a small-chord wing.

2. For the supersonic transport and for the slot drags incurred in this investigation, engine bleed air does not provide sufficient mass flow to warrant the use of air injection over an entire wing span. However, if the engine bleed air is injected only over the nacelles, it appears possible at Mach 2.0 to achieve a drag reduction equivalent to from 9 to 35 percent of the nacelle skin friction, the percentage depending on the amount of bleed plenum pressure energy that is used for thrust. Full recovery of the energy in the bleed plenum air amounts to an equivalent reduction in nacelle skin friction of 65 percent.

3. If a given quantity of gas must be ejected (for example, engine bleed air or spent cabin air), the greatest net drag reductions can be achieved by optimizing the slot drag and the available thrust rather than the skin-friction reduction.

4. Greater net drag reductions are obtained by injecting helium than by injecting air or Freon into the boundary layer, but calculations show that for a typical high-performance supersonic transport configuration, the increase in drag due to lift caused by the extra weight of the helium is greater than the skin-friction reduction.

5. The 0.004-chord rounded-shoulder slot achieved the greatest net drag reduction; but for a given slot-opening size, the sharp-shoulder slots, the screens, and the perforated plates seem to have lower slot drag.

6. The lift-interference effects of an injected gas should be considered in selecting the location of an ejection slot or nozzle on an aircraft.

Langley Research Center,
National Aeronautics and Space Administration,
Langley Station, Hampton, Va., April 8, 1969,
129-01-08-39-23.

REFERENCES

1. Clarke, Joseph H.; Menkes, Hans R.; and Libby, Paul A.: A Provisional Analysis of Turbulent Boundary Layers With Injection. J. Aeronaut. Sci., vol. 22, no. 4, Apr. 1955, pp. 255-260.

2. Dorrance, William H.; and Dore, Frank J.: The Effect of Mass Transfer on the Compressible Turbulent Boundary-Layer Skin Friction and Heat Transfer. J. Aeronaut. Sci., vol. 21, no. 6, June 1954, pp. 404-410.

3. Persh, Jerome: A Theoretical Investigation of the Effect of Injection of Air on Turbulent Boundary-Layer Skin-Friction and Heat-Transfer Coefficients at Supersonic and Hypersonic Speeds. NAVORD Rep. 4220, U.S. Naval Ord. Lab. (White Oak, Md.), Jan. 4, 1957.

4. Rubesin, Morris W.: An Analytical Estimation of the Effect of Transpiration Cooling on the Heat-Transfer and Skin-Friction Characteristics of a Compressible, Turbulent Boundary Layer. NACA TN 3341, 1954.

5. Tendeland, Thorval; and Okuno, Arthur F.: The Effect of Fluid Injection on the Compressible Turbulent Boundary Layer – The Effect on Skin Friction of Air Injected into the Boundary Layer of a Cone at M = 2.7. NACA RM A56D05, 1956.

6. Dershin, Harvey; Leonard, Charles A.; and Gallaher, William H.: Direct Measurement of Skin Friction on a Porous Flat Plate With Mass Injection. AIAA J., vol. 5, no. 11, Nov. 1967, pp. 1934-1939.

7. McRee, Donald I.; Peterson, John B., Jr.; and Braslow, Albert L.: Effect of Air Injection Through a Porous Surface and Through Slots on Turbulent Skin Friction at Mach 3. NASA TN D-2427, 1964.

8. Peterson, John B., Jr.; McRee, Donald I.; Adcock, Jerry B.; and Braslow, Albert L.: Further Investigation of Effect of Air Injection Through Slots and Porous Surfaces on Flat-Plate Turbulent Skin Friction at Mach 3. NASA TN D-3311, 1966.

9. Czarnecki, K. R.: Analytical Investigation of Reduction in Turbulent Skin Friction on a Flat Plate by Means of Air Injection Through Discrete Slots. NASA TN D-2102, 1964.

10. Mechtly, E. A.: The International System of Units – Physical Constants and Conversion Factors. NASA SP-7012, 1964.

11. Sommer, Simon C.; and Short, Barbara J.: Free-Flight Measurements of Turbulent-Boundary-Layer Skin Friction in the Presence of Severe Aerodynamic Heating at Mach Numbers From 2.8 to 7.0. NACA TN 3391, 1955.

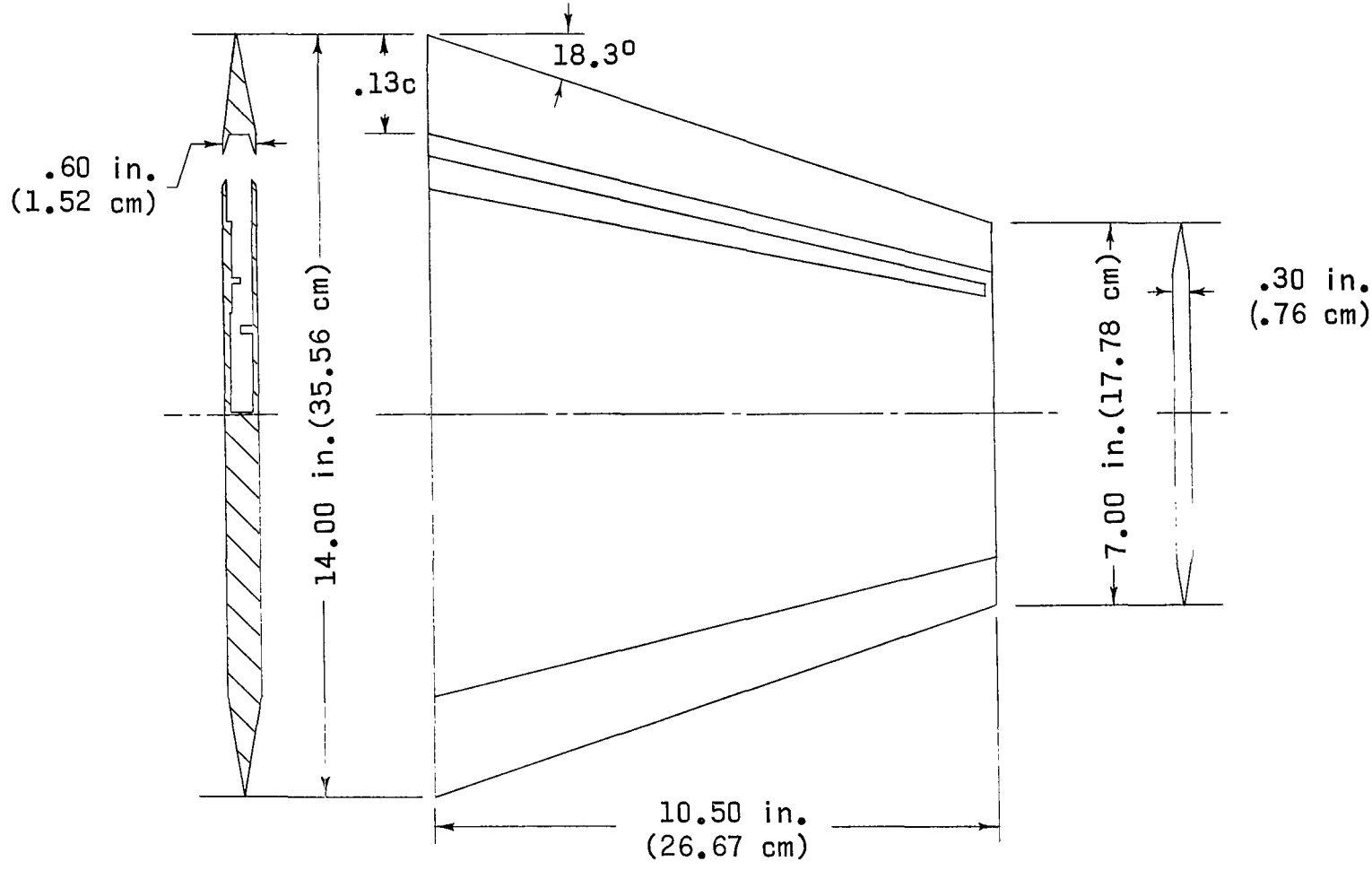

Figure 1.- Wing planform and sections.

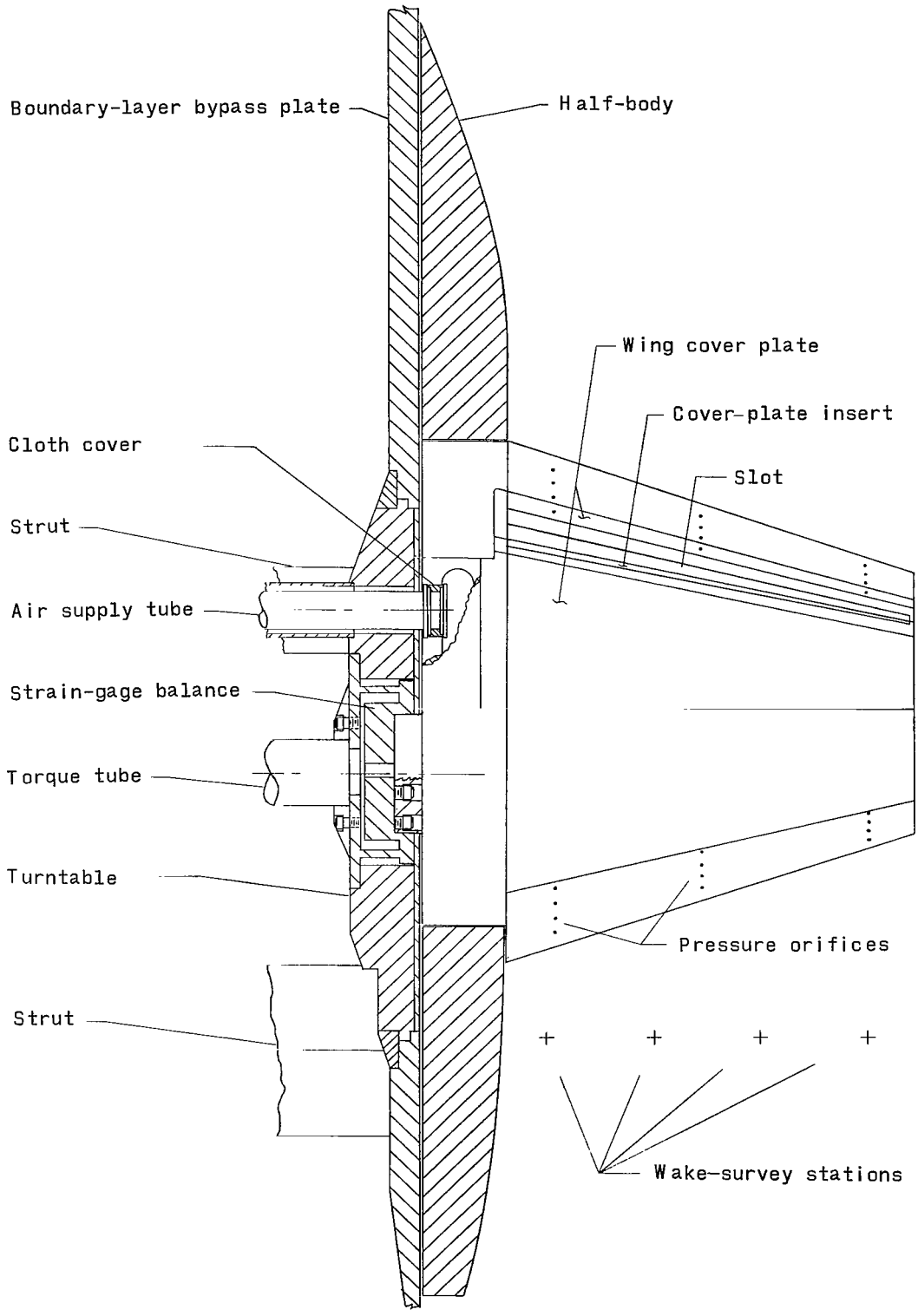

Figure 2.- Model installation.

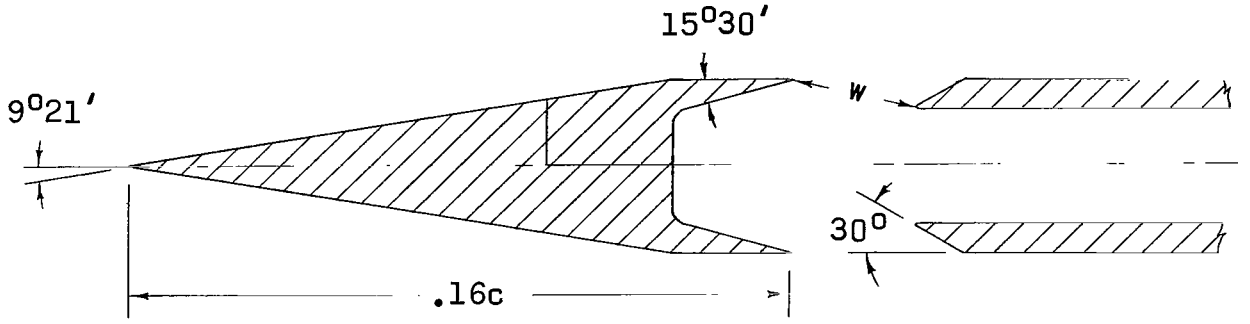

(a) Sharp-shoulder slots.

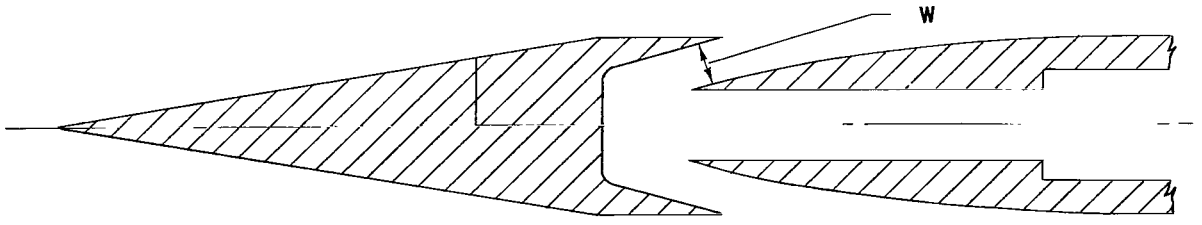

(b) Rounded-shoulder slots.

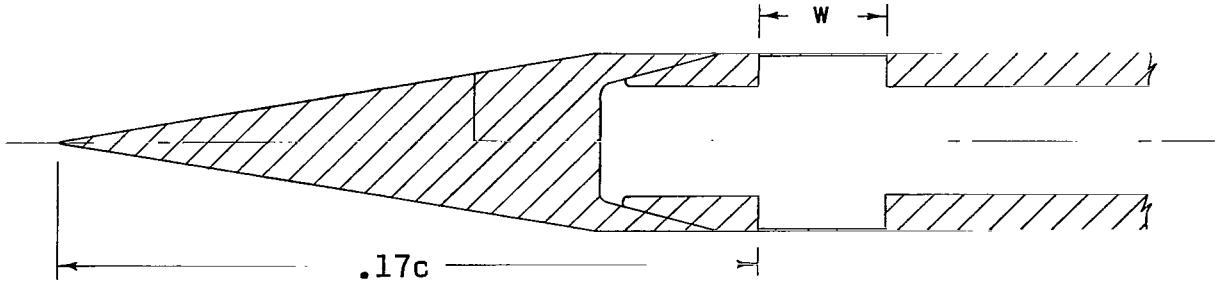

(c) Screens and perforated plates.

Figure 3.- Three basic slot configurations.

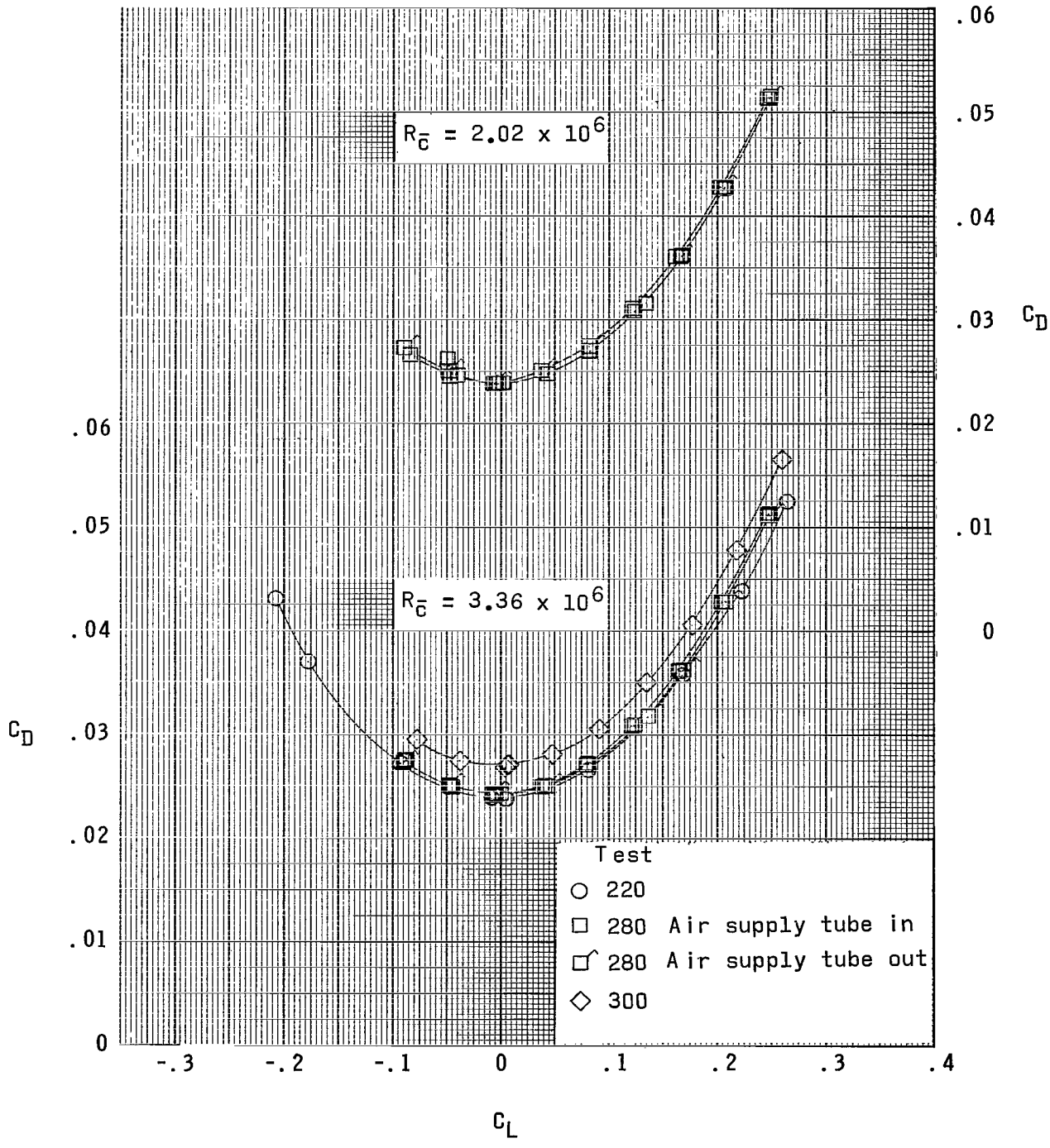

Figure 4.- Measured lift-drag data of the smooth wing.

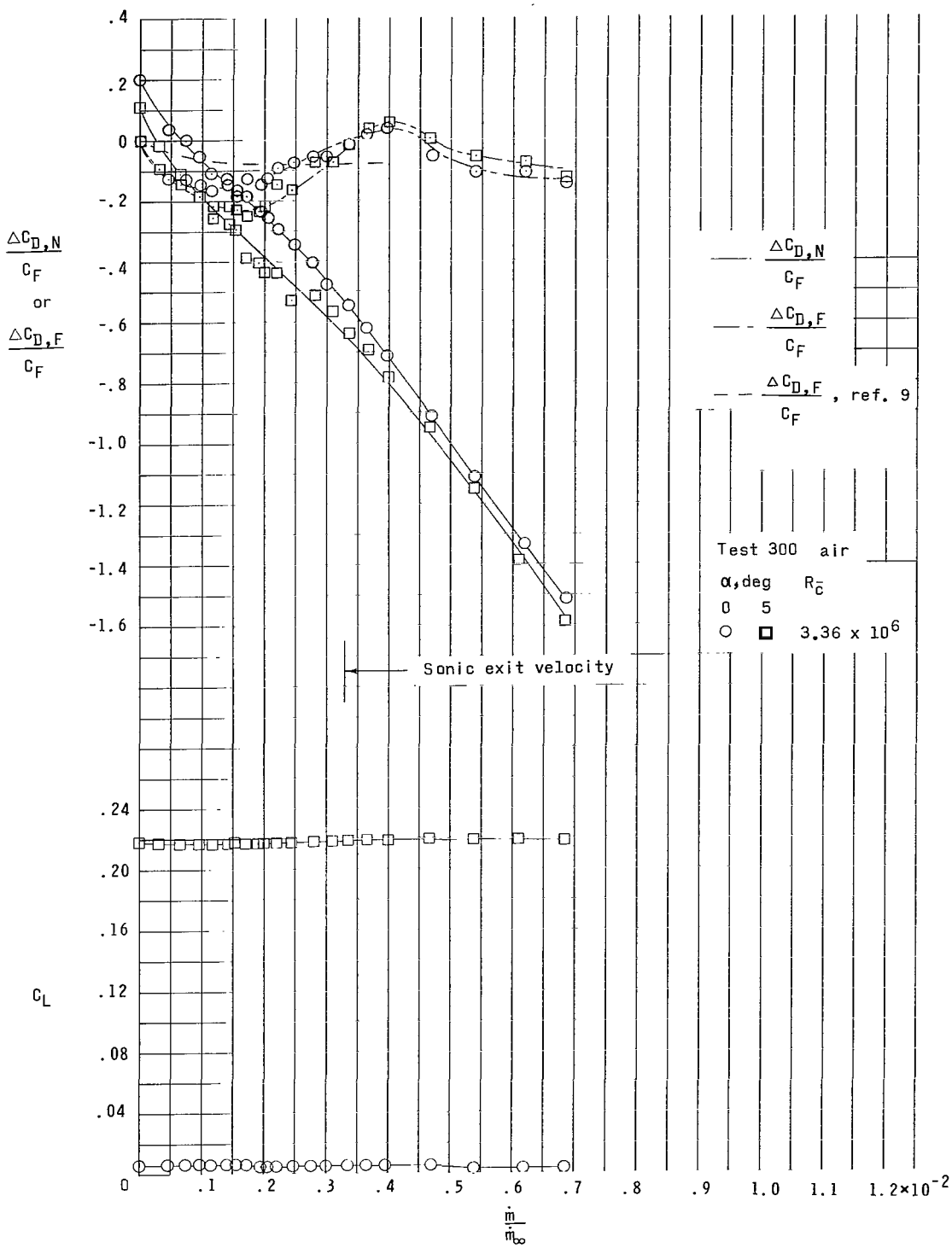

(a) w = 0.004c rounded-shoulder slot on top and bottom surfaces.

Figure 5.- Variation of drag reduction ratios and lift coefficient with mass-flow ratio.

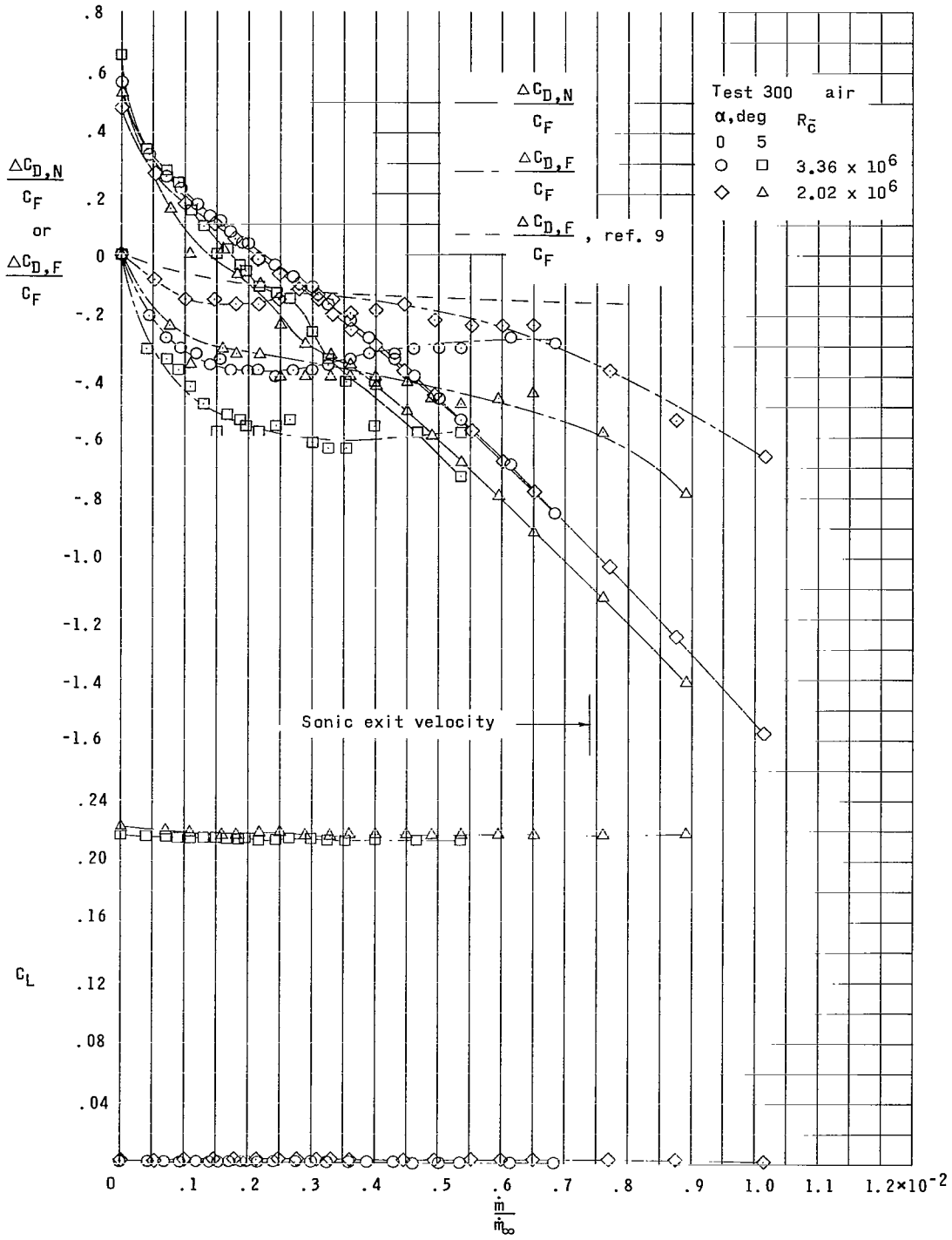

(b) w = 0.009c rounded-shoulder slot on top and bottom surfaces.

Figure 5.- Continued.

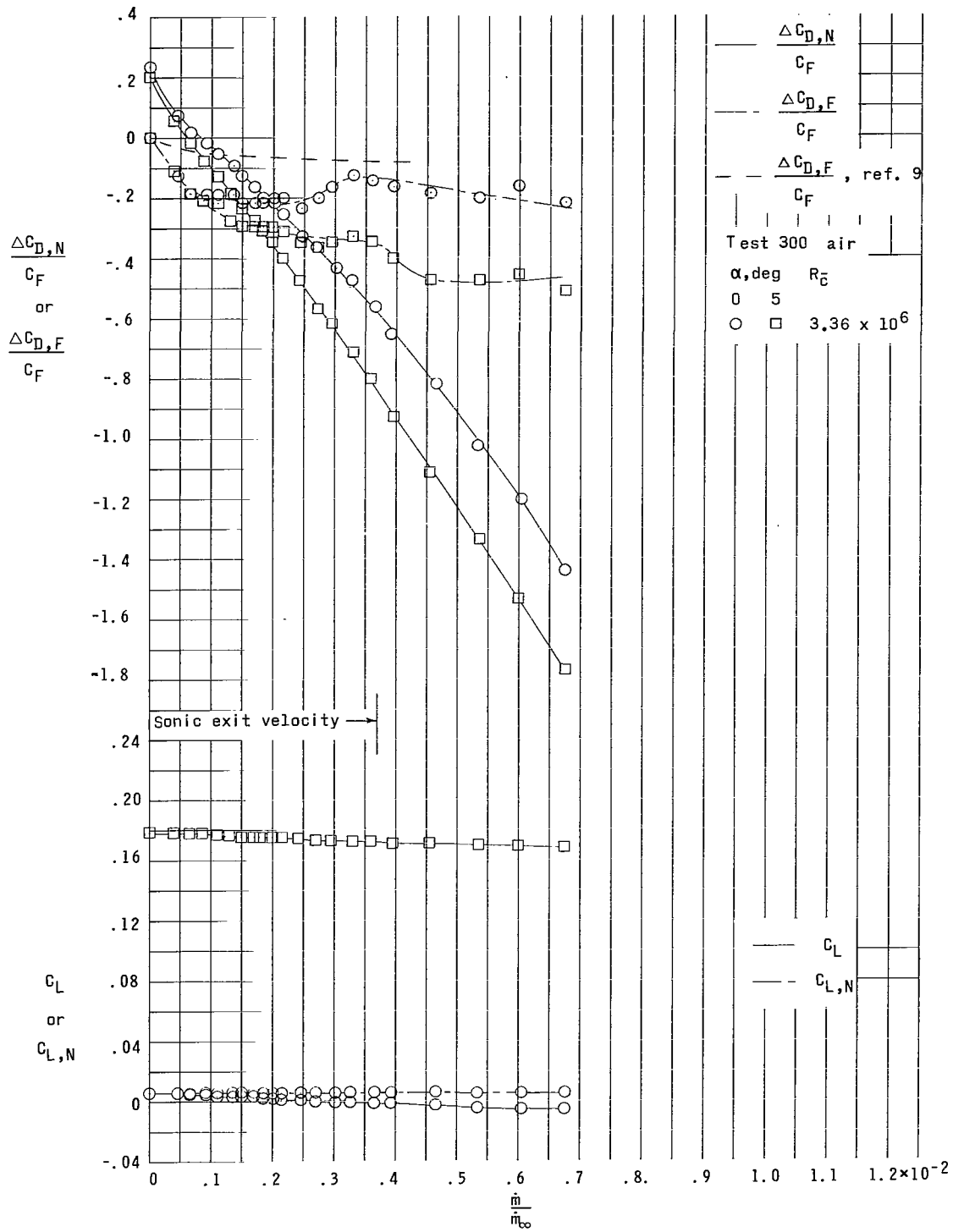

(c) w = 0.009c rounded-shoulder slot on top surface; bottom surface smooth.

Figure 5.- Continued.

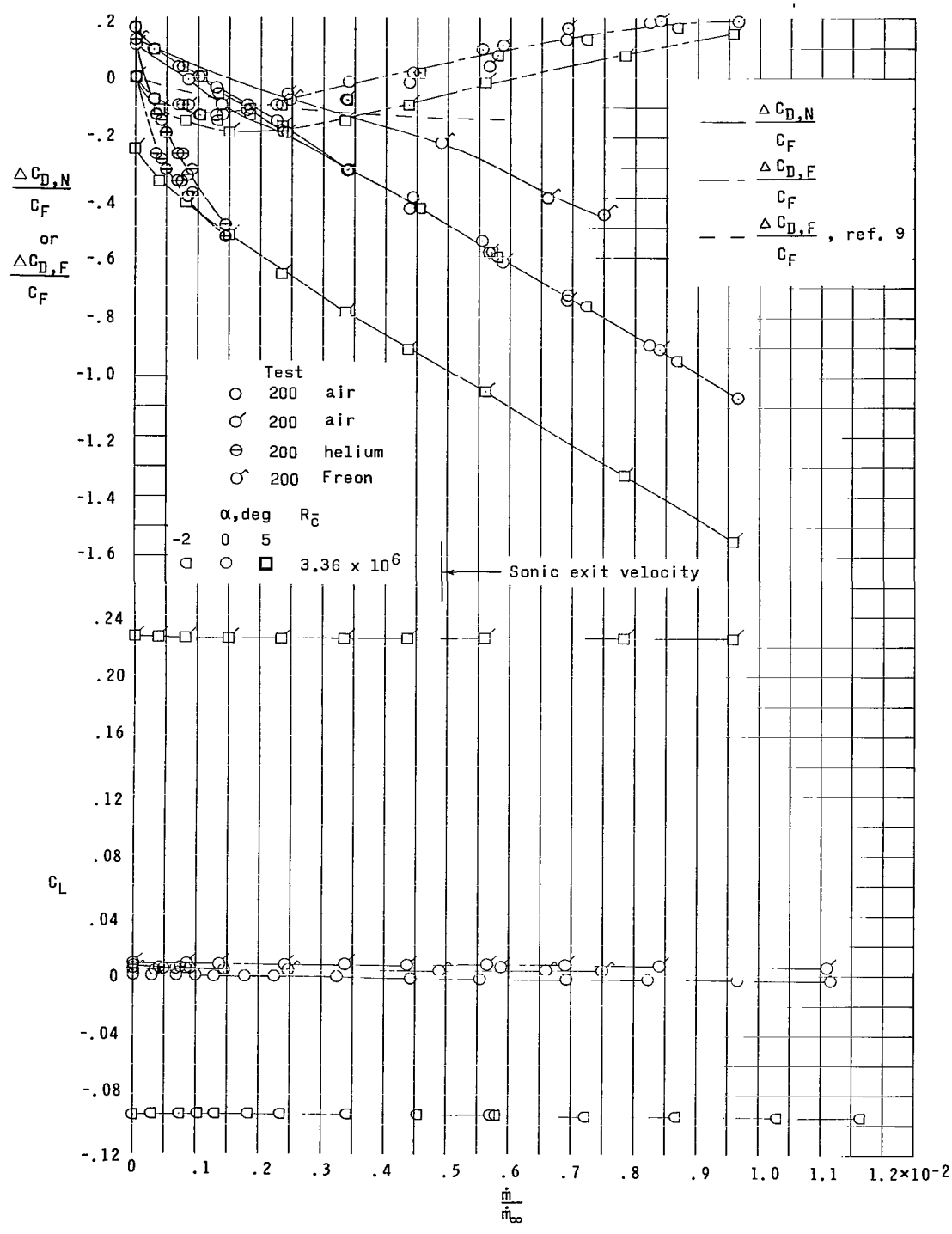

(d) w = 0.006c sharp-shoulder slot on top and bottom surfaces.

Figure 5.- Continued.

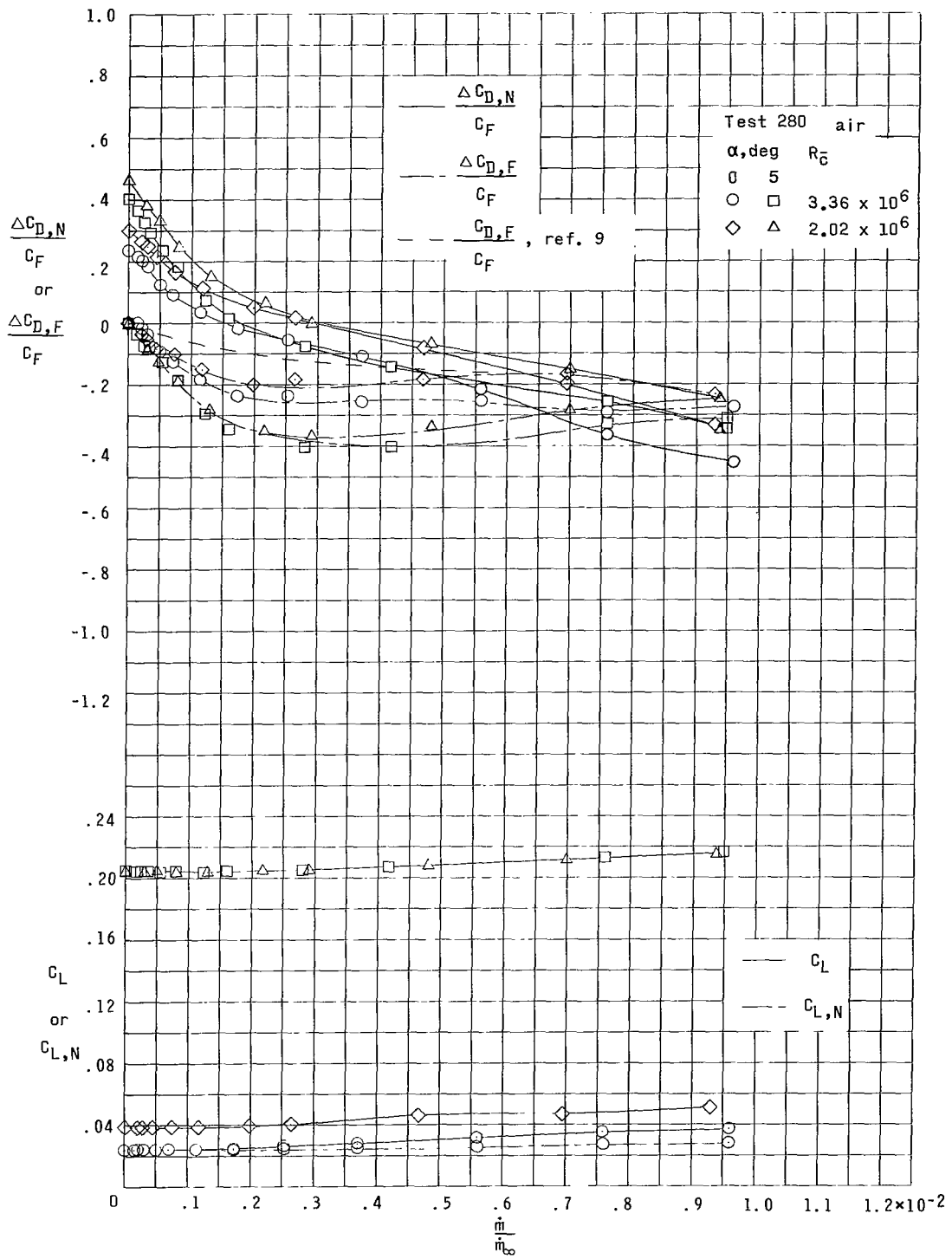

(e) w = 0.006c sharp-shoulder slot on top surface; w = 0.03c sharp-shoulder slot on bottom surface.

Figure 5.- Continued.

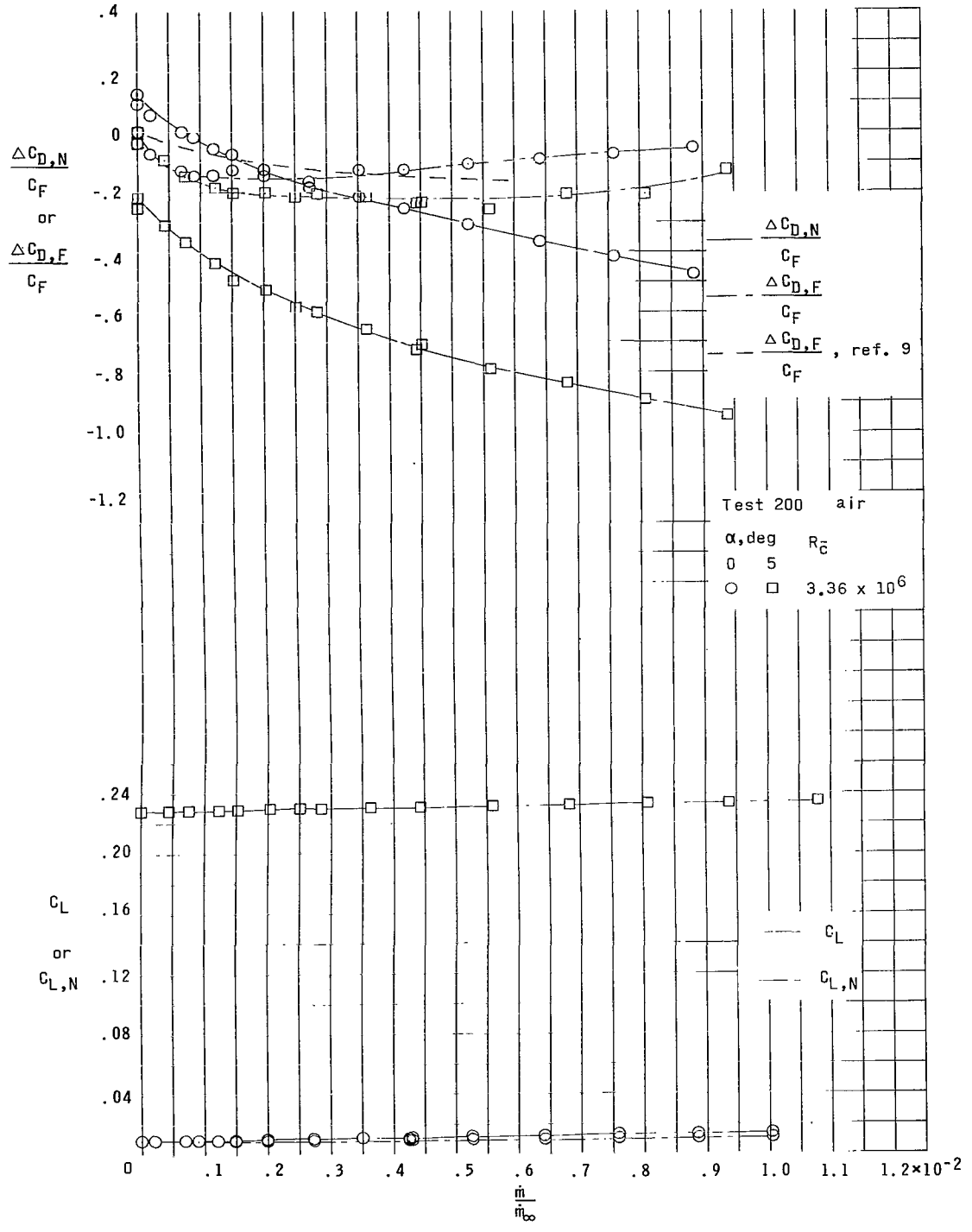

(f) w = 0.006c sharp-shoulder slot on top surface; w = 0.026c screen (100 × 100 per in^2 (39.4 × 39.4 per cm^2) mesh) on bottom surface.

Figure 5.- Continued.

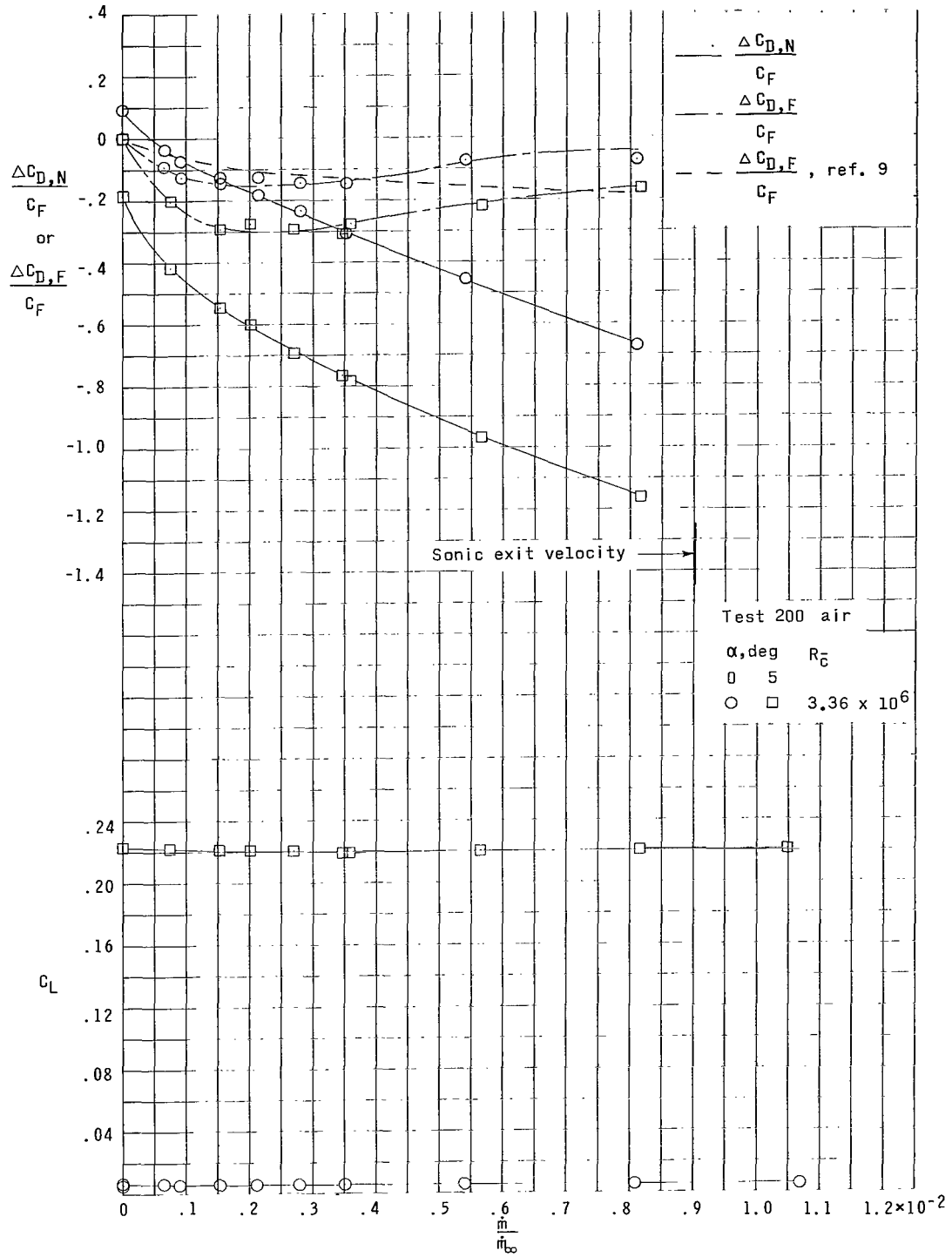

(g) w = 0.011c sharp-shoulder slot on top and bottom surfaces.

Figure 5.- Continued.

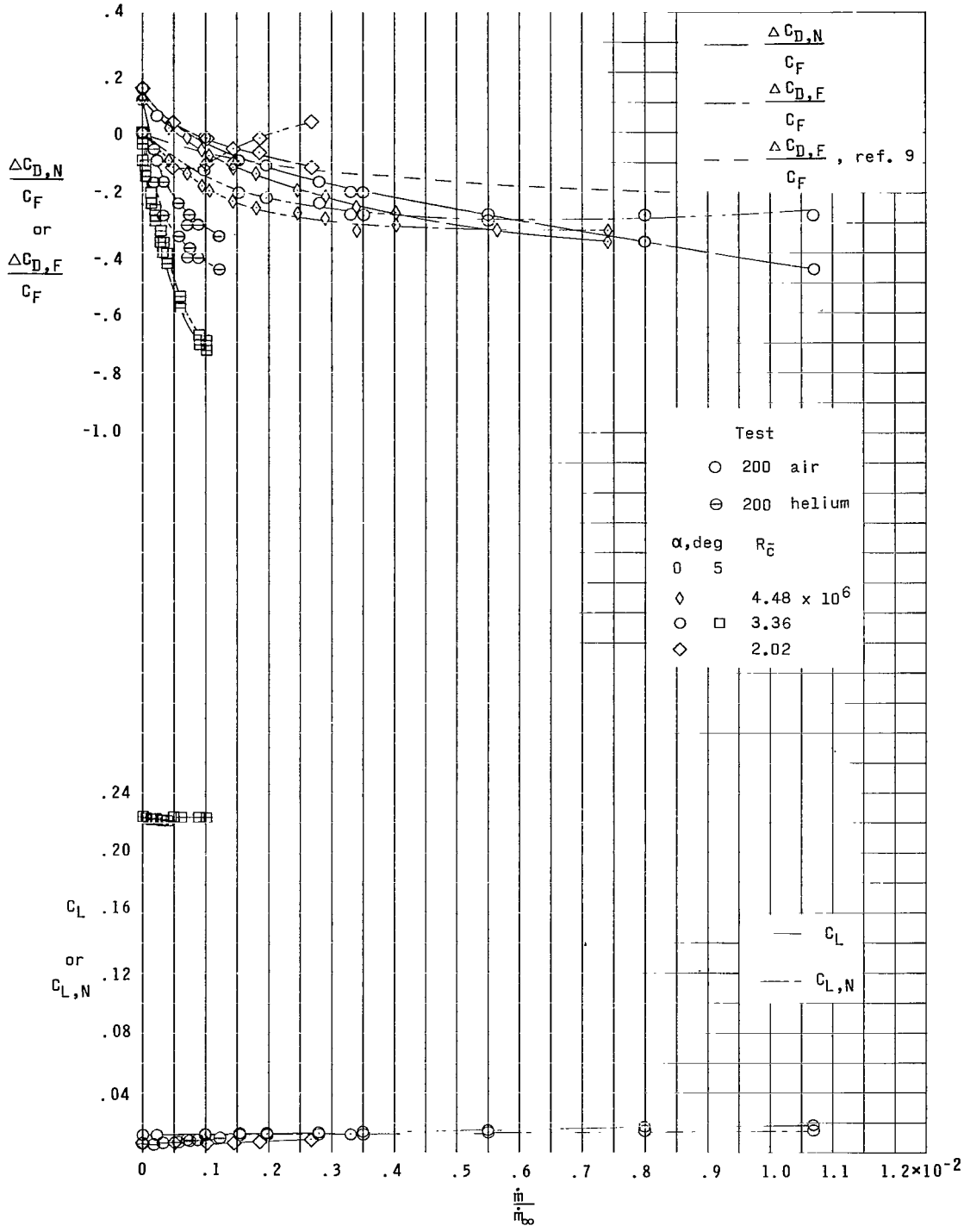

(h) w = 0.011c sharp-shoulder slot on top surface; w = 0.03c sharp-shoulder slot on bottom surface.

Figure 5.- Continued.

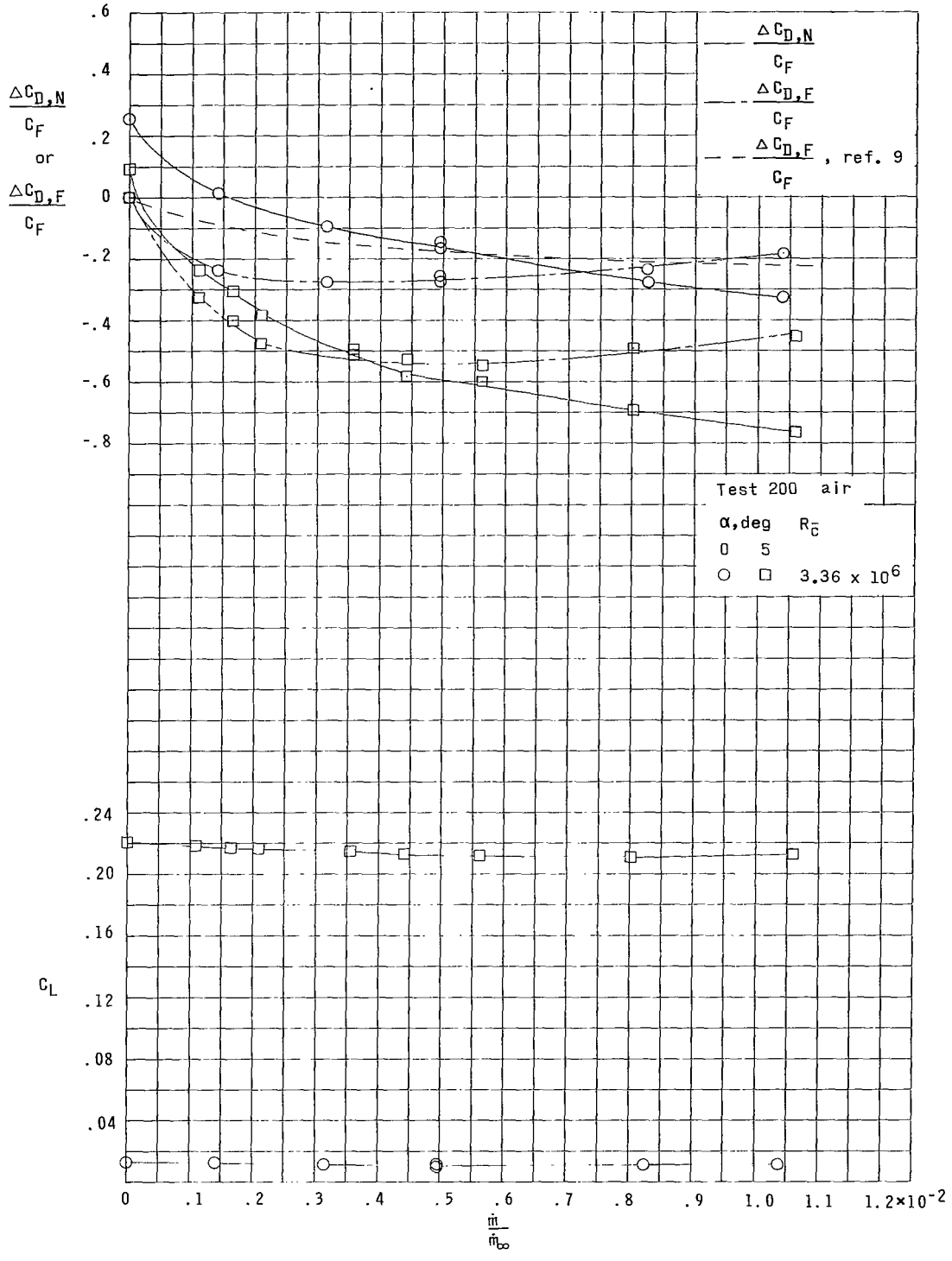

(i) w = 0.019c sharp-shoulder slot on top and bottom surfaces.

Figure 5.- Continued.

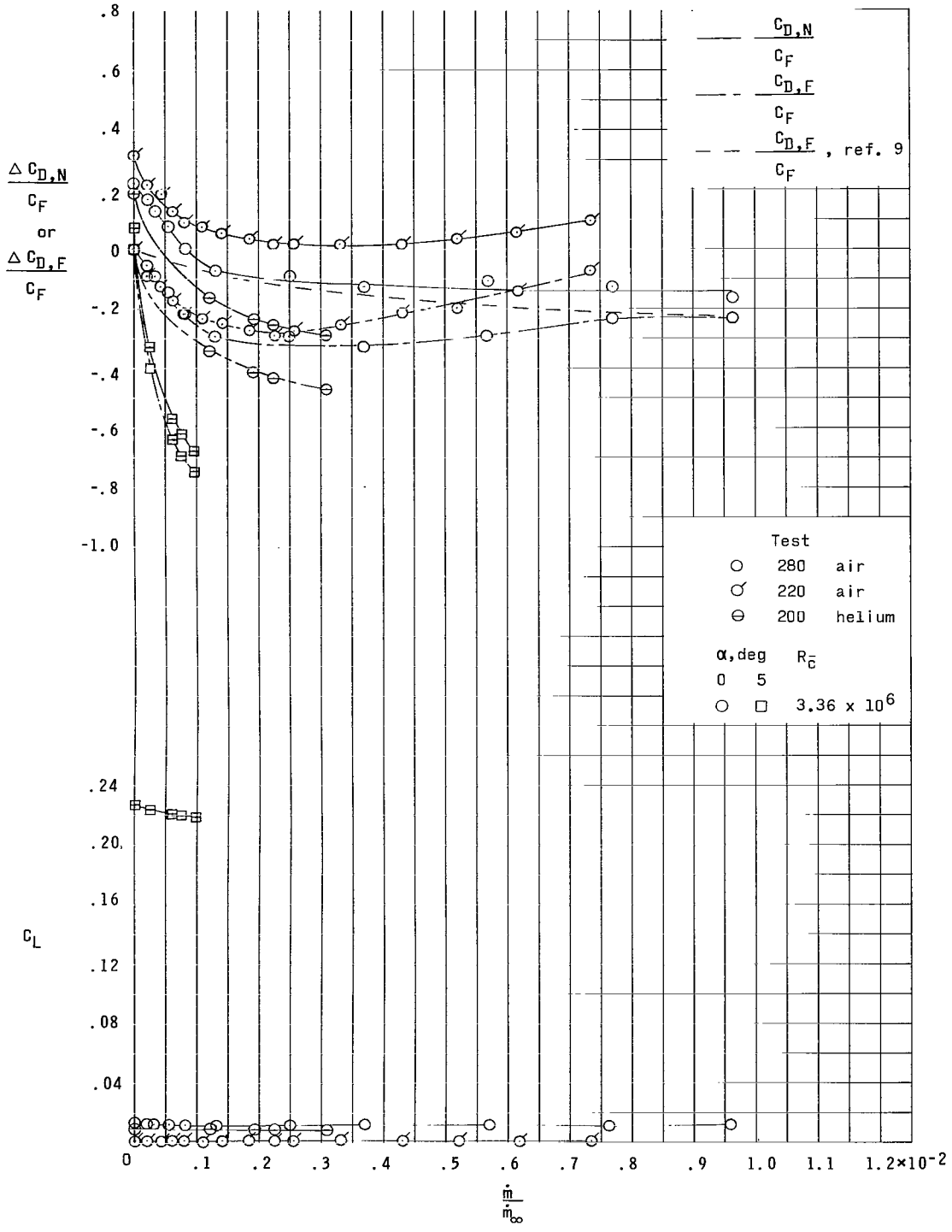

(j) w = 0.03c sharp-shoulder slot on top and bottom surfaces.

Figure 5.- Continued.

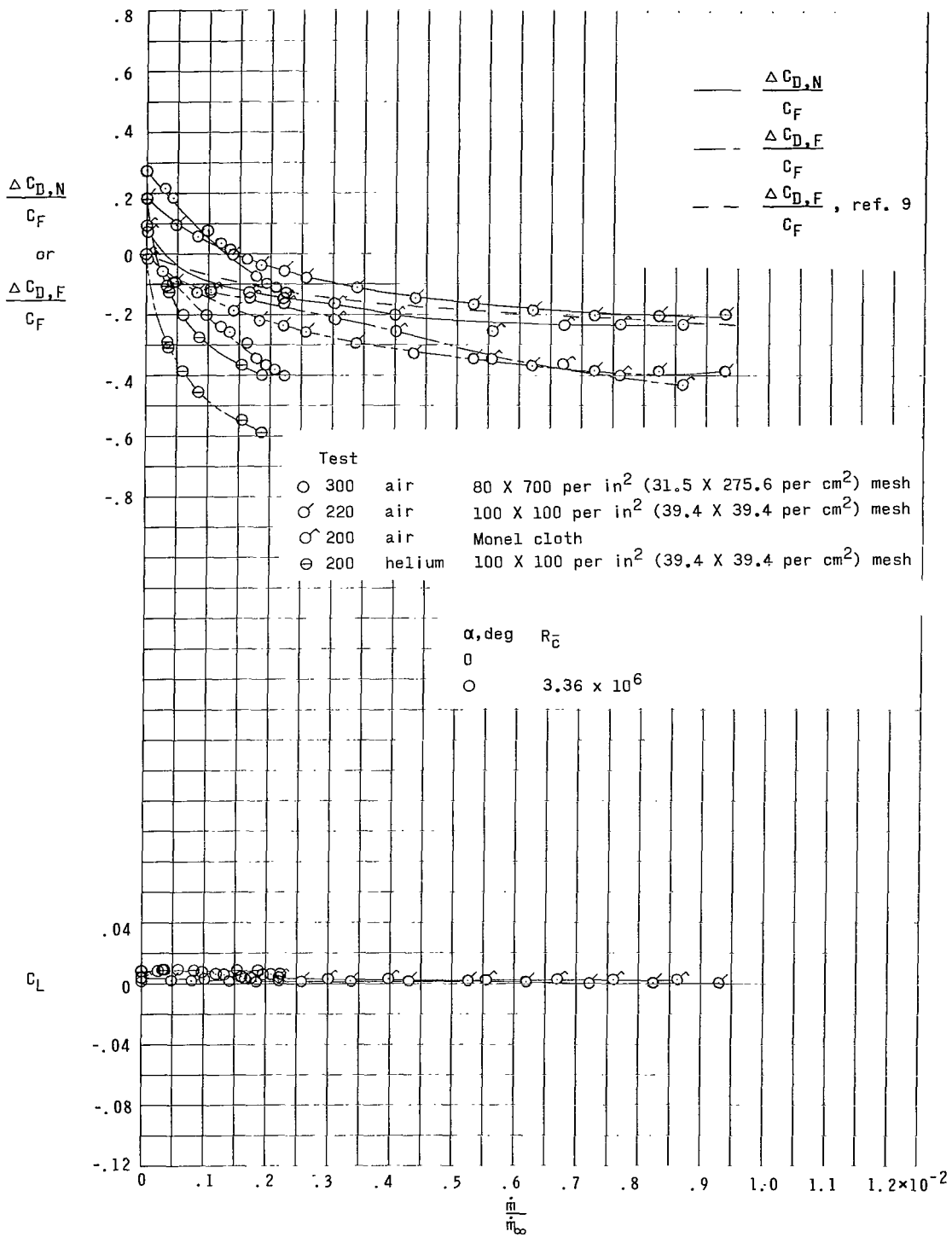

(k) w = 0.026c screen (100 × 100 per in^2 (39.4 × 39.4 per cm^2) mesh) on top and bottom surfaces.

Figure 5.- Continued.

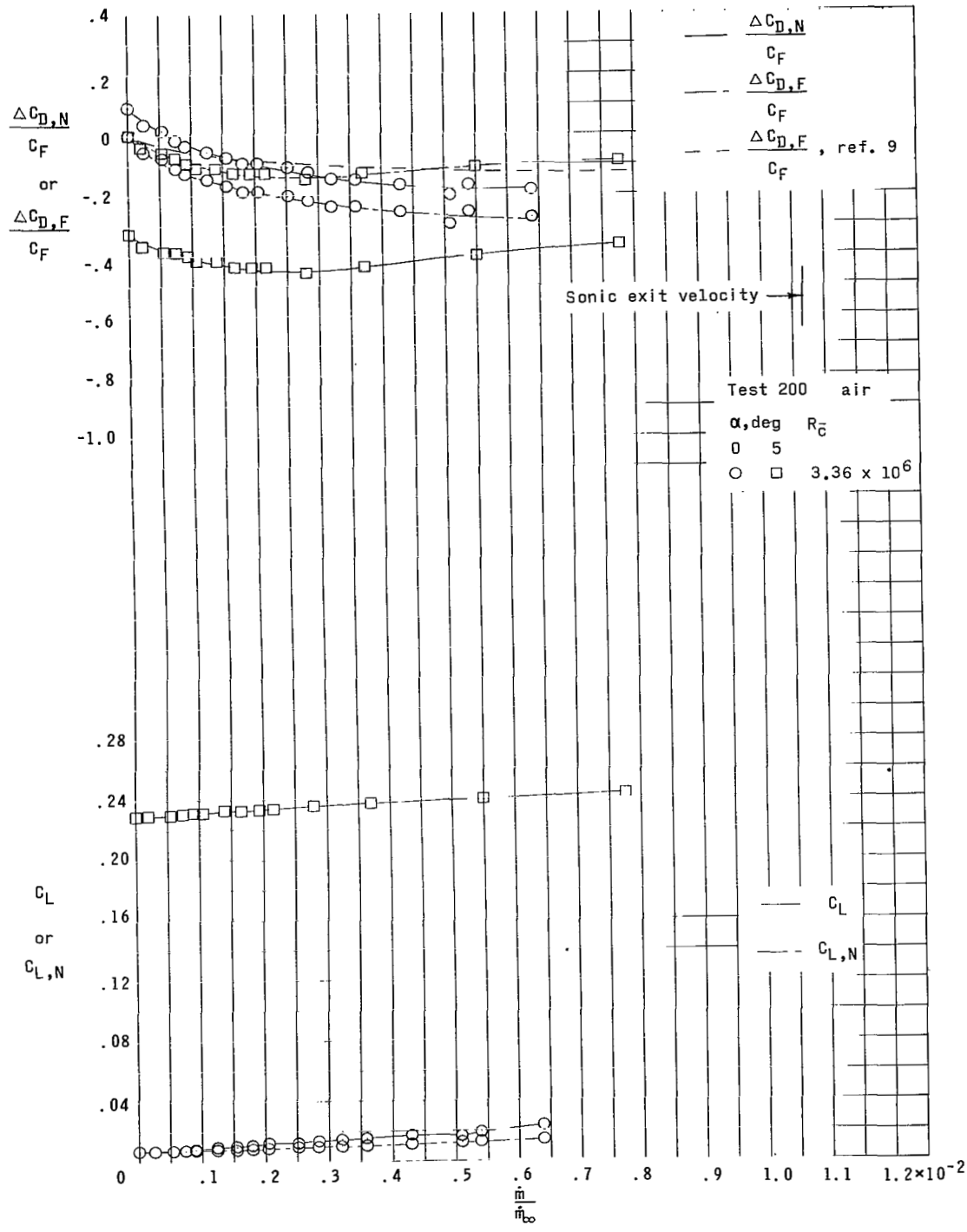

(l) Top surface smooth; w = 0.026c screen (100 × 100 per in^2 (39.4 × 39.4 cm^2) mesh) on bottom surface.

Figure 5.- Continued.

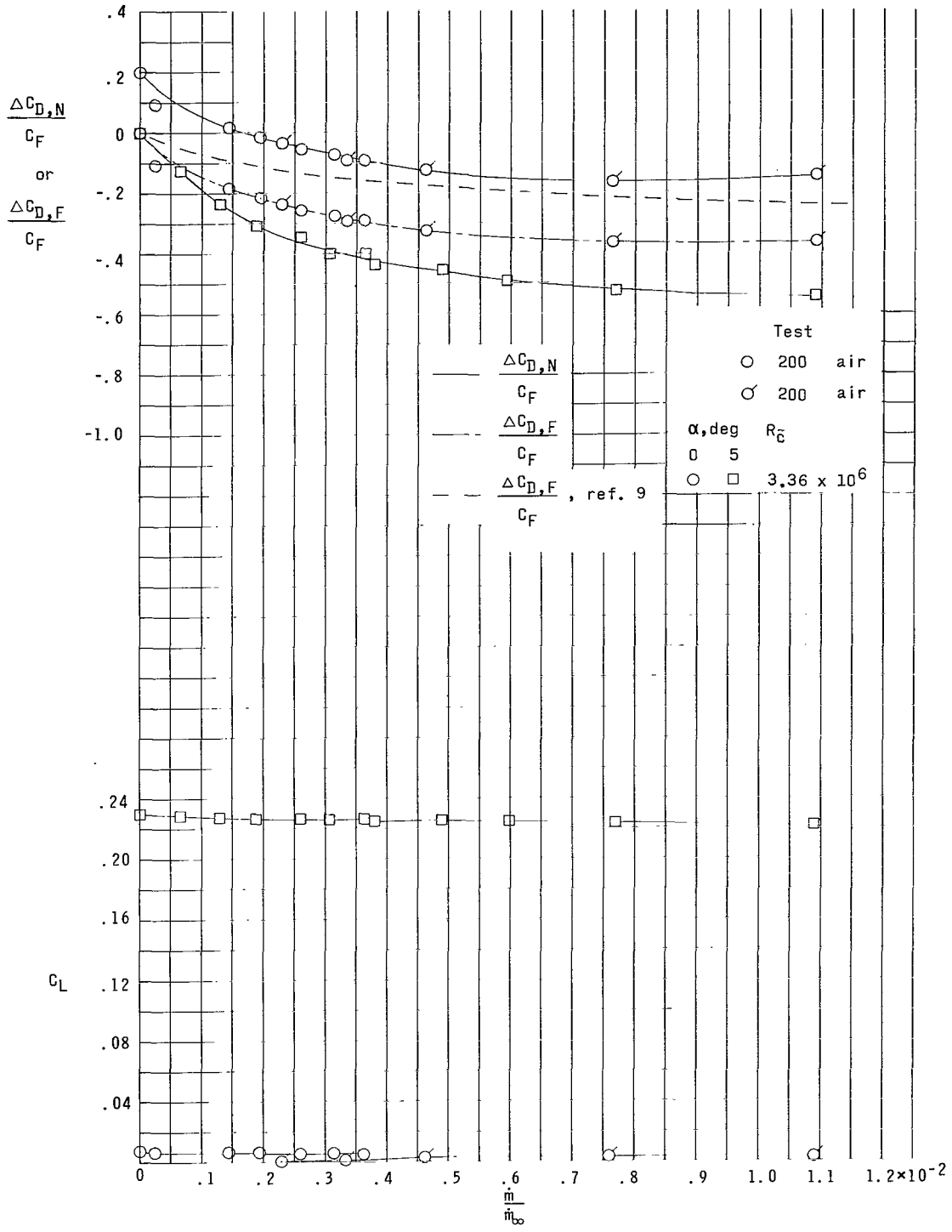

(m) w = 0.026c screen (100 × 100 per in^2 (39.4 × 39.4 per cm^2) mesh) on inboard half of wing; smooth surface on outboard half of wing.

Figure 5.- Continued.

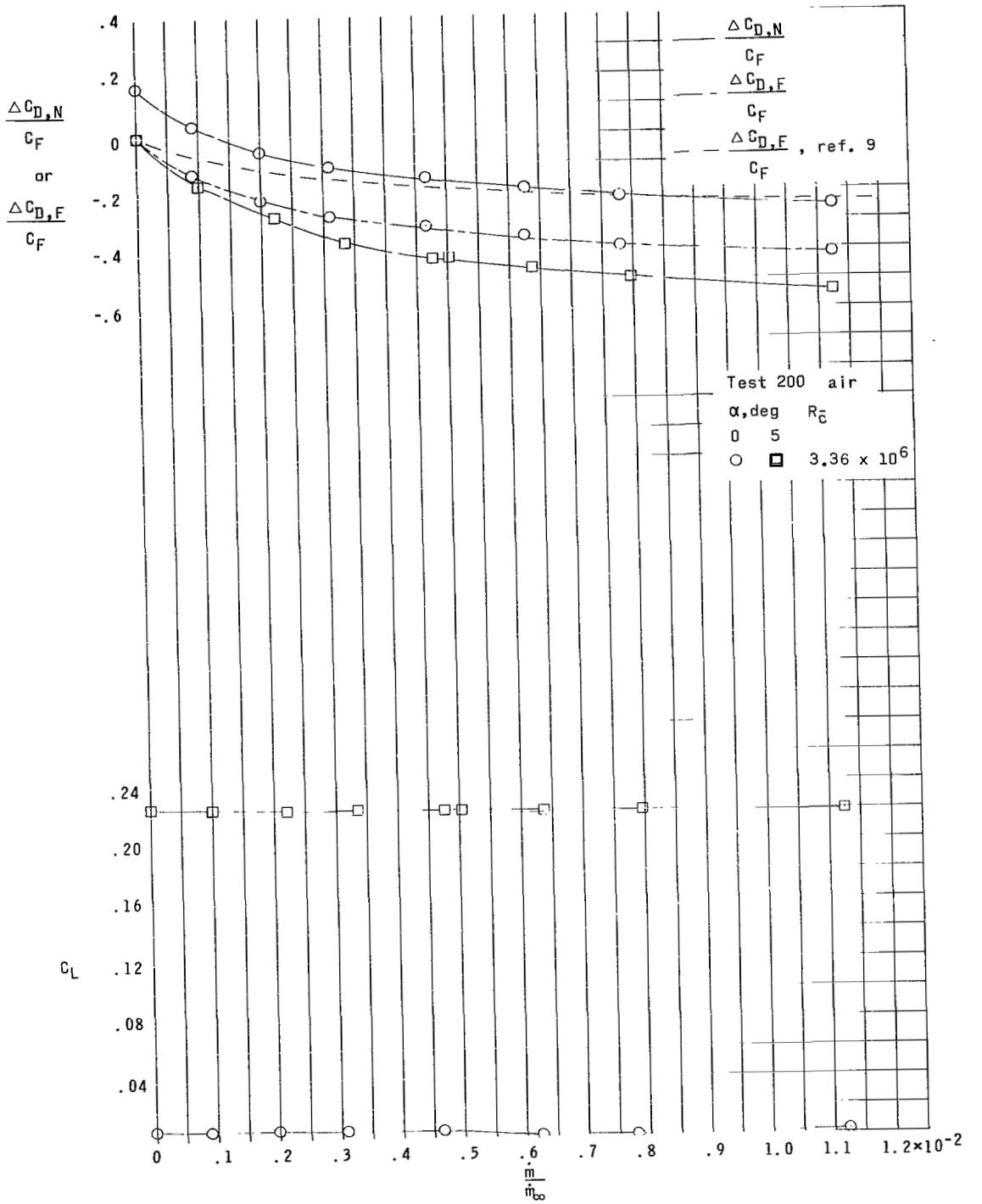

(n) w = 0.026c screen (100 × 100 per in^2 (39.4 × 39.4 per cm^2) mesh) on outboard half of wing; smooth surface on inboard half of wing.

Figure 5.- Continued.

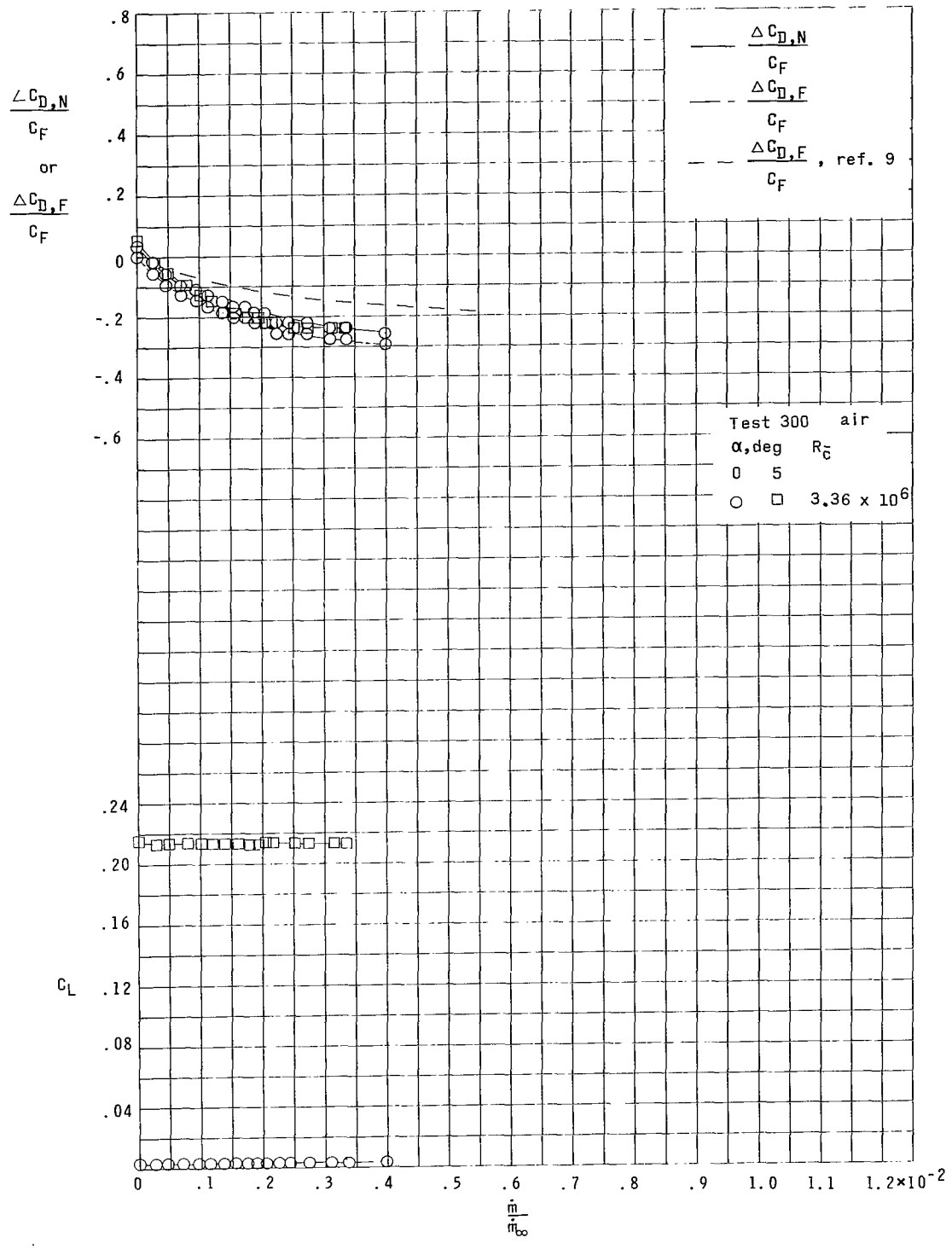

(o) w = 0.059c screen (80 × 700 per in^2 (31.5 × 275.6 per cm^2) mesh) on top and bottom surfaces.

Figure 5.- Continued.

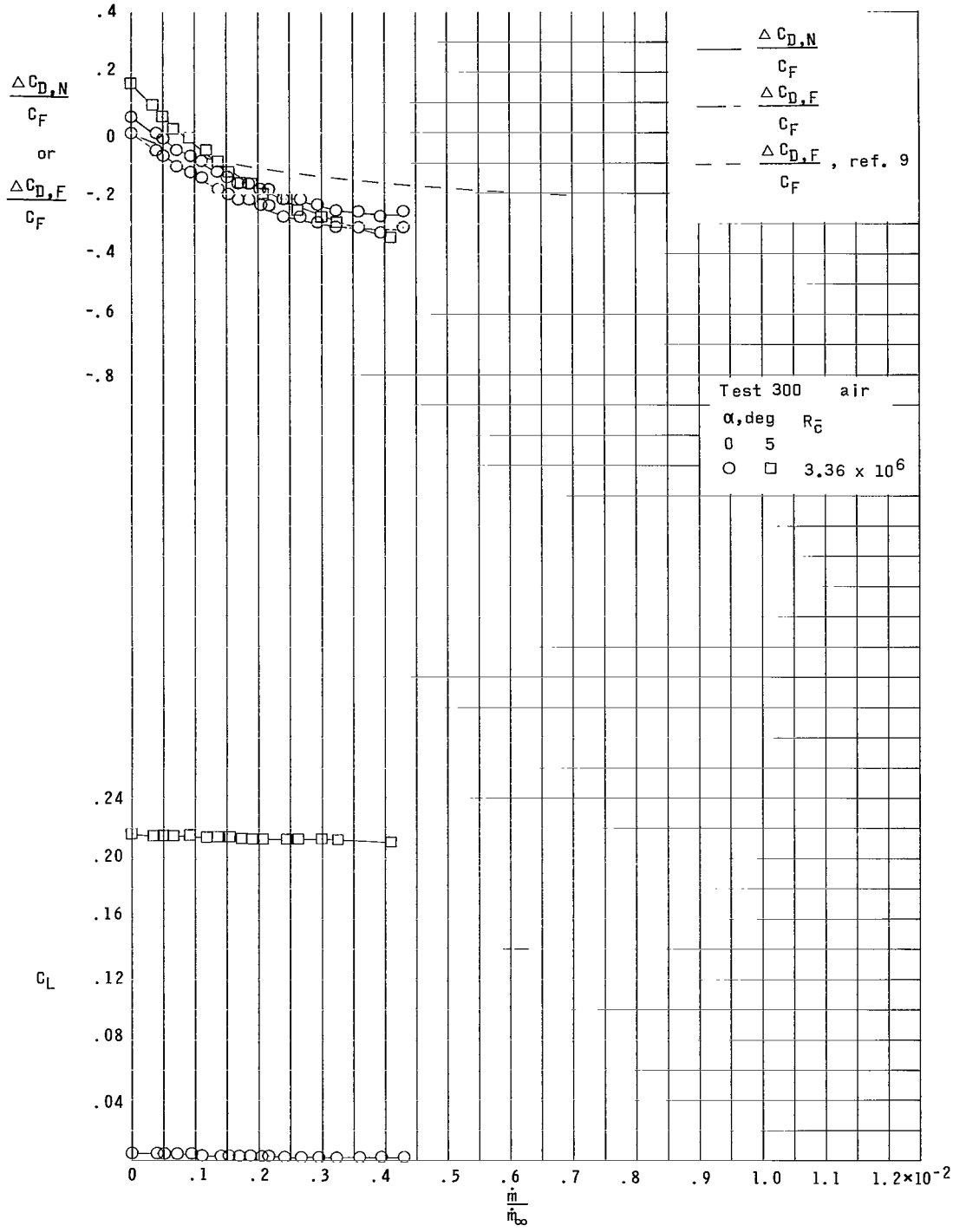

(p) w = 0.116c screen on top surface; w = 0.059c screen on bottom surface (both screens 80 × 700 per in^2 (31.5 × 275.6 per cm^2) mesh).

Figure 5.- Continued.

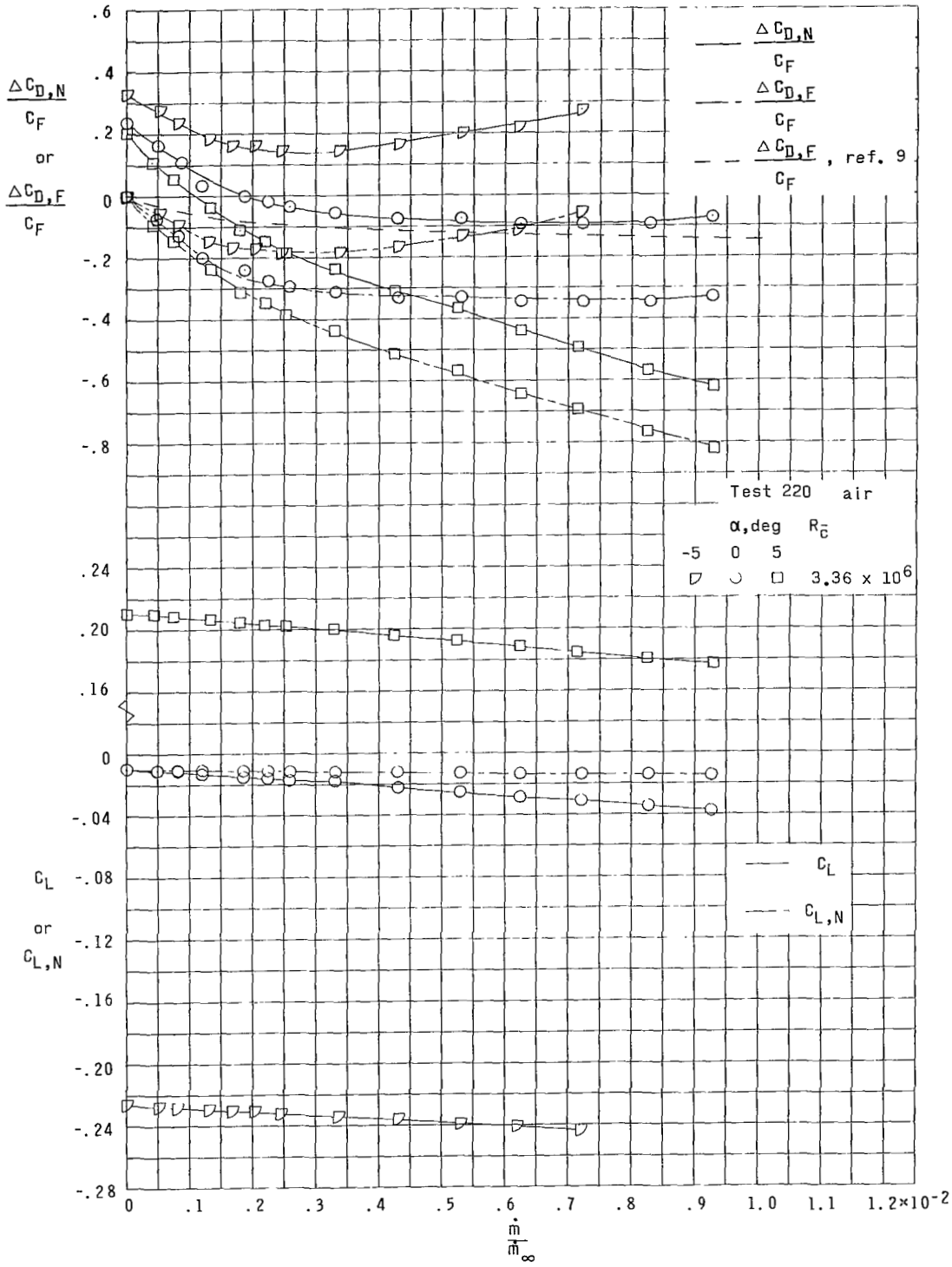

(q) w = 0.116c screen (100 × 100 per in^2 (39.4 × 39.4 per cm^2) mesh) on top surface; bottom surface smooth.

Figure 5.- Continued.

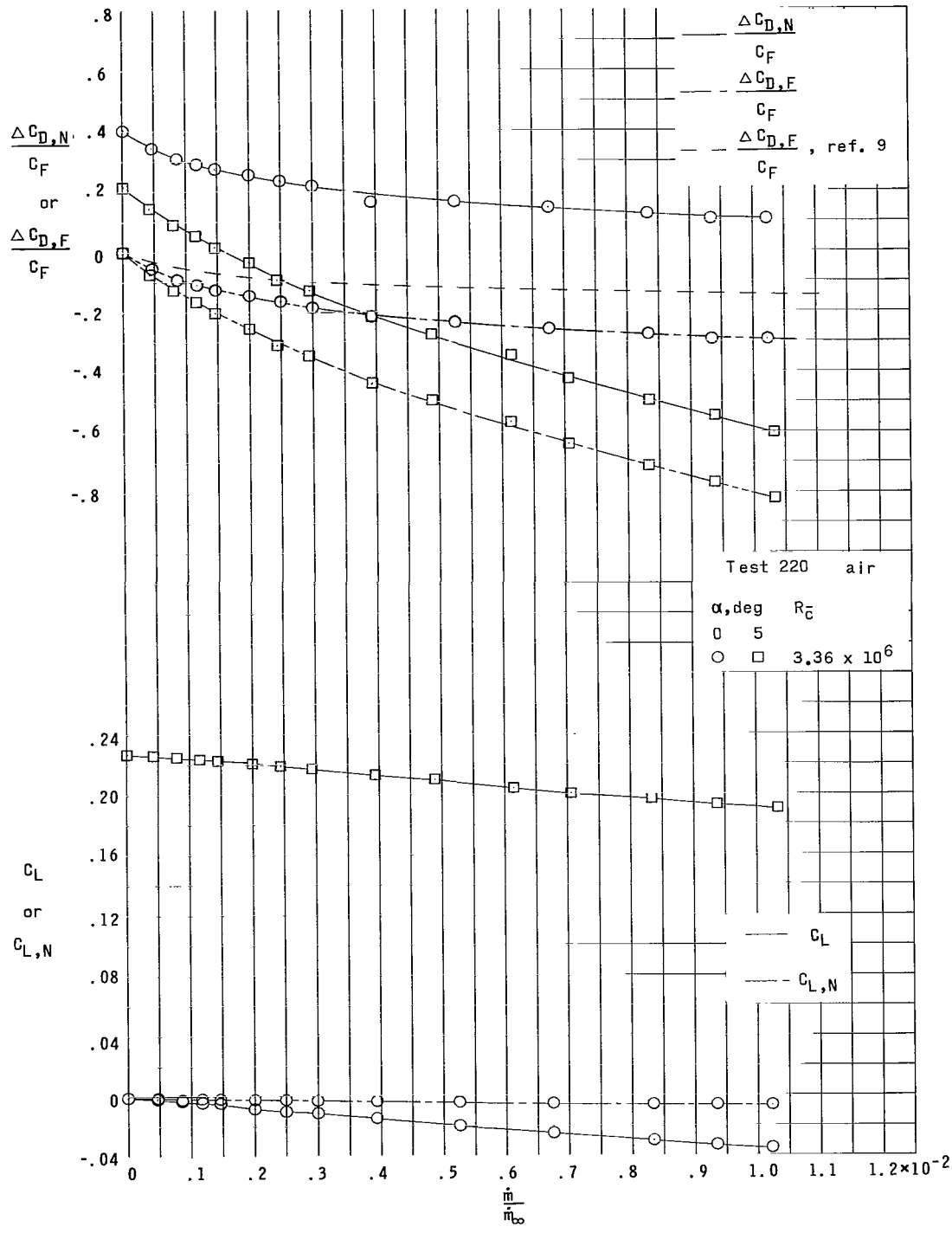

(r) w = 0.227c screen (100 × 100 per in^2 (39.4 × 39.4 per cm^2) mesh) on top surface; bottom surface smooth.

Figure 5.- Continued.

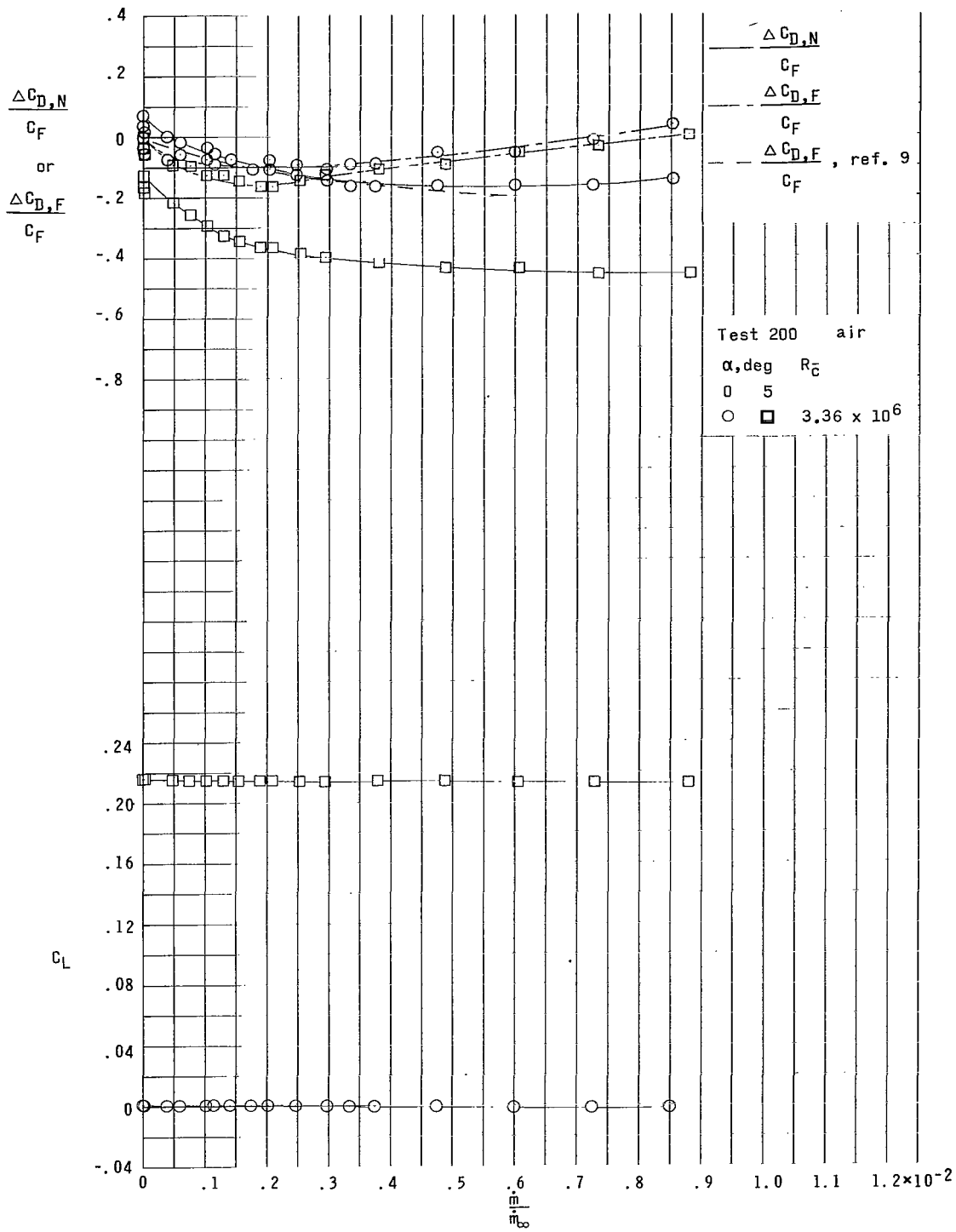

(s) w = 0.026c perforated plate on top and bottom surfaces.

Figure 5.- Continued.

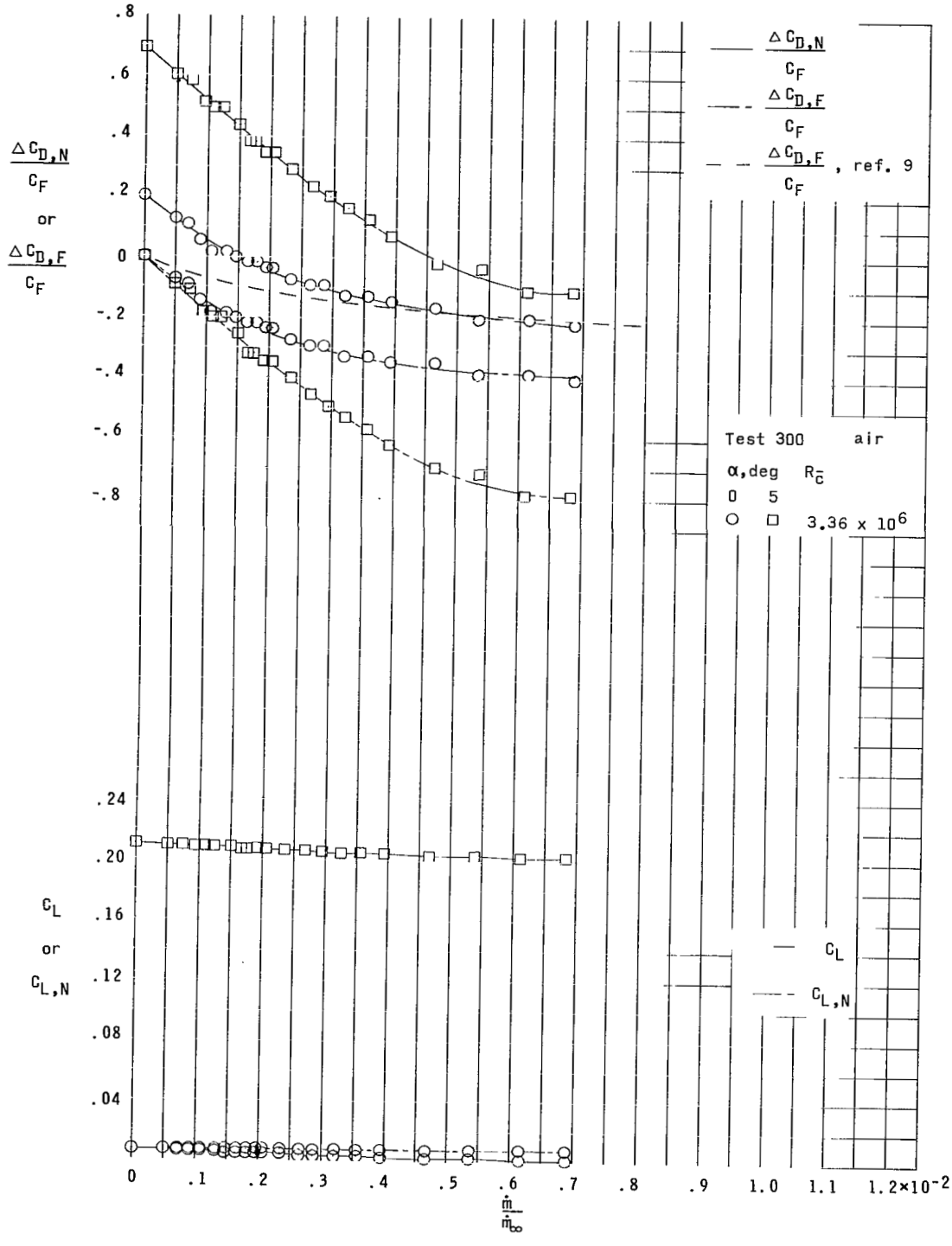

(t) w = 0.116c perforated plate on top surface; w = 0.026c perforated plate on bottom surface.

Figure 5.- Concluded.

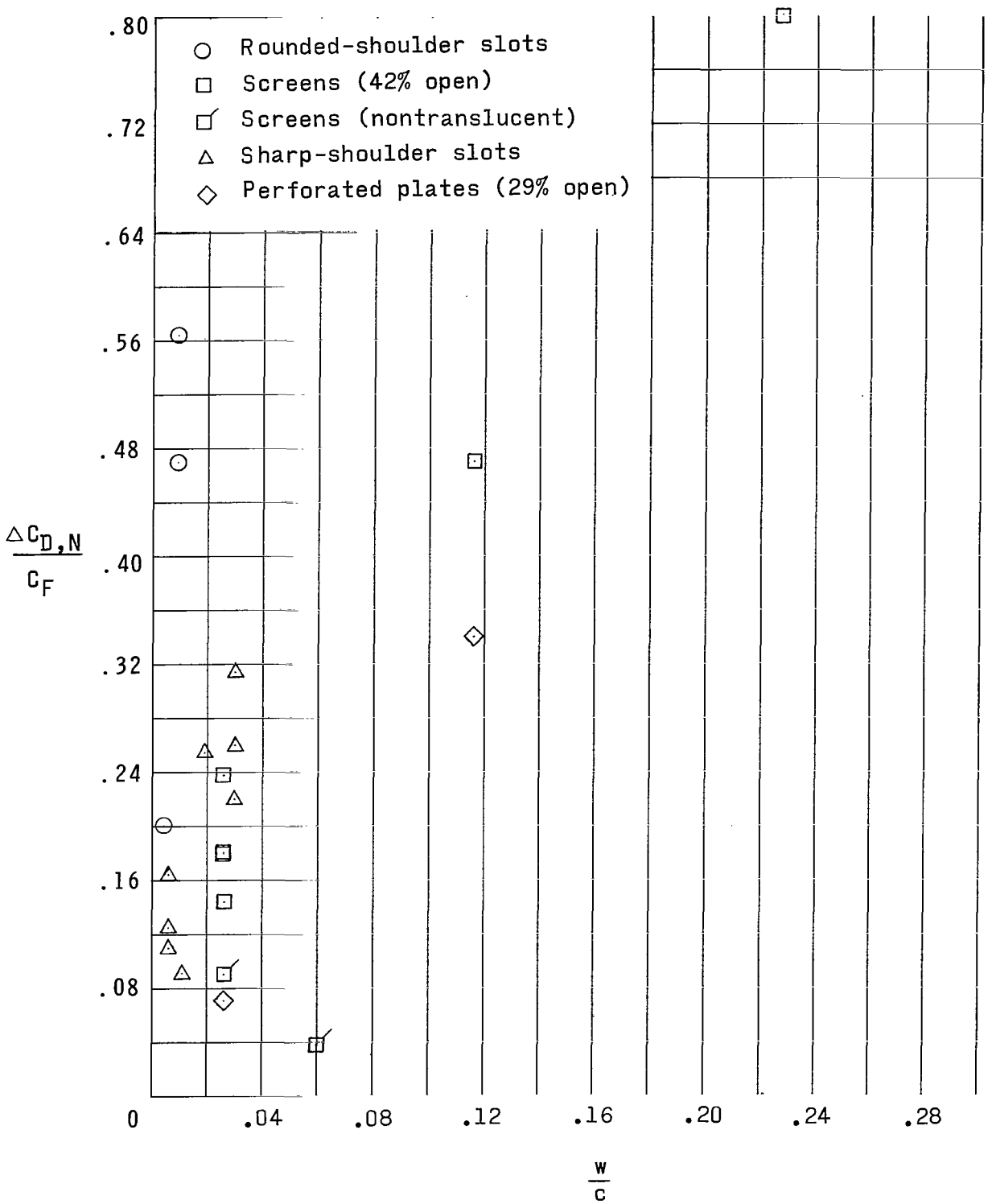

Figure 6.- Zero-mass-flow slot drags at $\alpha = 0^0$ (slots on both upper and lower surfaces).

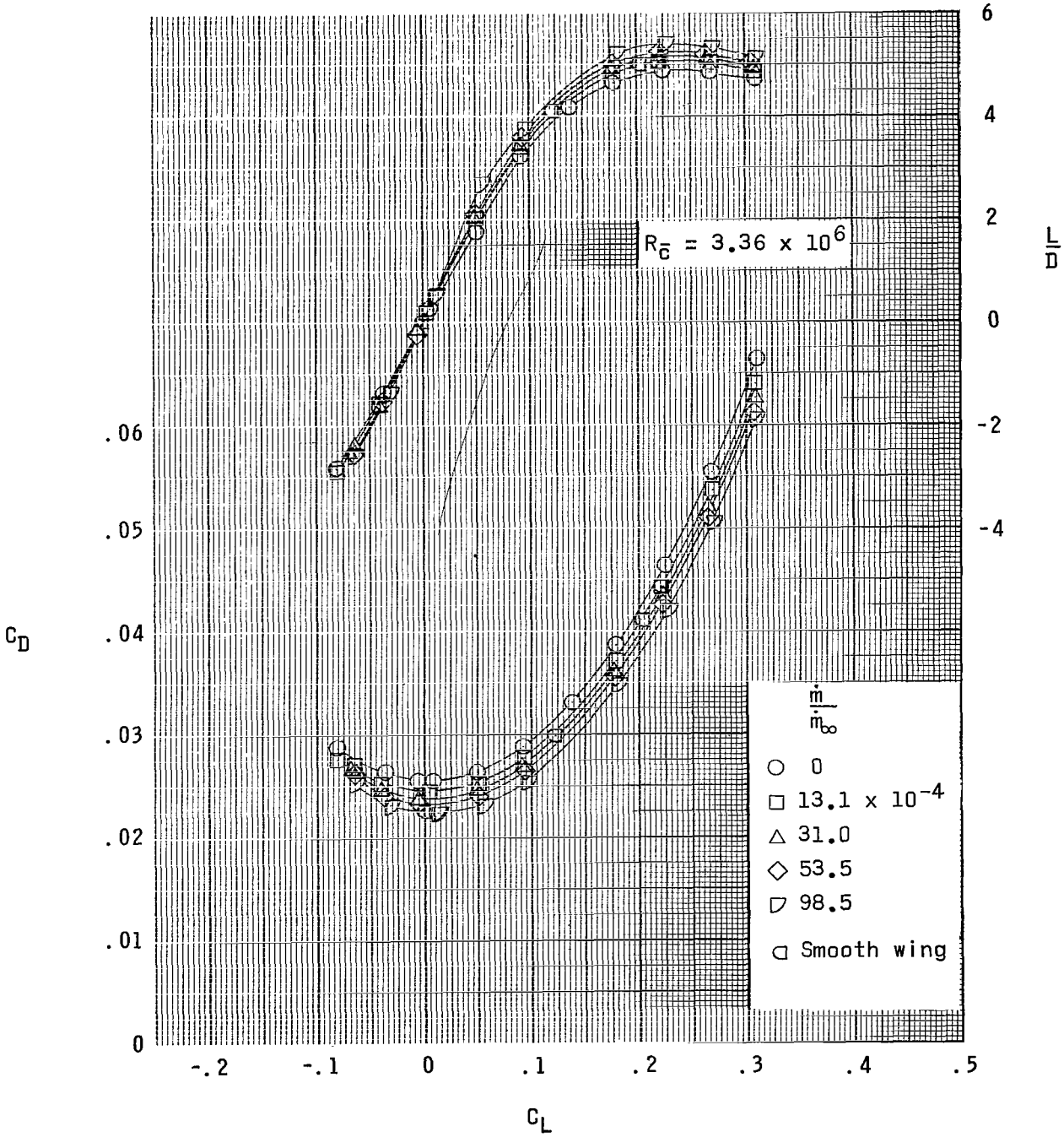

Figure 7.- Effect of mass-flow ratio on the lift-drag data with w = 0.011c sharp-shoulder slot on top surface and w = 0.03c sharp-shoulder slot on bottom surface.

NATIONAL AERONAUTICS AND SPACE ADMINISTRATION
WASHINGTON, D. C. 20546
OFFICIAL BUSINESS

FIRST CLASS MAIL

POSTAGE AND FEES PAID
NATIONAL AERONAUTICS AND
ION

POSTMASTER: If Undeliverable (Section 158 Postal Manual) Do Not Return

"The aeronautical and space activities of the United States shall be conducted so as to contribute . . . to the expansion of human knowledge of phenomena in the atmosphere and space. The Administration shall provide for the widest practicable and appropriate dissemination of information concerning its activities and the results thereof."

—NATIONAL AERONAUTICS AND SPACE ACT OF 1958

NASA SCIENTIFIC AND TECHNICAL PUBLICATIONS

TECHNICAL REPORTS: Scientific and technical information considered important, complete, and a lasting contribution to existing knowledge.

TECHNICAL NOTES: Information less broad in scope but nevertheless of importance as a contribution to existing knowledge.

TECHNICAL MEMORANDUMS: Information receiving limited distribution because of preliminary data, security classification, or other reasons.

CONTRACTOR REPORTS: Scientific and technical information generated under a NASA contract or grant and considered an important contribution to existing knowledge.

TECHNICAL TRANSLATIONS: Information published in a foreign language considered to merit NASA distribution in English.

SPECIAL PUBLICATIONS: Information derived from or of value to NASA activities. Publications include conference proceedings, monographs, data compilations, handbooks, sourcebooks, and special bibliographies.

TECHNOLOGY UTILIZATION PUBLICATIONS: Information on technology used by NASA that may be of particular interest in commercial and other non-aerospace applications. Publications include Tech Briefs, Technology Utilization Reports and Notes, and Technology Surveys.

Details on the availability of these publications may be obtained from:

SCIENTIFIC AND TECHNICAL INFORMATION DIVISION

NATIONAL AERONAUTICS AND SPACE ADMINISTRATION

Washington, D.C. 20546